



Search for new physics with the M_{T2} variable in all-jets final states produced in pp collisions at $\sqrt{s} = 13$ TeV

The CMS Collaboration*

Abstract

A search for new physics is performed using events that contain one or more jets, no isolated leptons, and a large transverse momentum imbalance, as measured through the M_{T2} variable, which is an extension of the transverse mass in events with two invisible particles. The results are based on a sample of proton-proton collisions collected at a center-of-mass energy of 13 TeV with the CMS detector at the LHC, and that corresponds to an integrated luminosity of 2.3 fb^{-1} . The observed event yields in the data are consistent with predictions for the standard model backgrounds. The results are interpreted using simplified models of supersymmetry and are expressed in terms of limits on the masses of potential new colored particles. Assuming that the lightest neutralino is stable and has a mass less than about 500 GeV, gluino masses up to 1550–1750 GeV are excluded at 95% confidence level, depending on the gluino decay mechanism. For the scenario of direct production of squark-antisquark pairs, top squarks with masses up to 800 GeV are excluded, assuming a 100% branching fraction for the decay to a top quark and neutralino. Similarly, bottom squark masses are excluded up to 880 GeV, and masses of light-flavor squarks are excluded up to 600–1260 GeV, depending on the degree of degeneracy of the squark masses.

Published in the Journal of High Energy Physics as doi:10.1007/JHEP10(2016)006.

1 Introduction

Searches for new physics based on final states with jets and large transverse momentum imbalance are sensitive to broad classes of new physics models, including supersymmetry (SUSY) [1–8]. Such searches were previously conducted by both the CMS [9–13] and ATLAS [14, 15] collaborations, using data from 8 TeV proton-proton (pp) collisions. They placed lower limits on the masses of pair-produced colored particles near the TeV scale for a broad range of production and decay scenarios and provided some of the most stringent constraints on the production of supersymmetric particles. These searches are particularly interesting at this time as they are among the first to benefit from the increase in the CERN LHC center-of-mass energy from 8 to 13 TeV, as shown in two recent analyses of these final states by ATLAS and CMS [16, 17]. As a consequence of the increase in parton luminosity at 13 TeV, the cross section for the pair production of particles with the color quantum numbers of a gluon increases by more than a factor of 30 for a particle of mass 1.5 TeV.

In this paper we present results of a search for new physics in events with jets and significant transverse momentum imbalance, as characterized by the “stransverse mass” M_{T2} , a kinematic variable that was first proposed for use in SUSY searches in Refs. [18, 19] and used in several Run 1 searches [13, 20]. The search is performed using a data sample corresponding to an integrated luminosity of 2.3 fb^{-1} of pp collisions collected at a center-of-mass energy of 13 TeV with the CMS detector at the LHC.

In this analysis we select events with at least one jet and veto events with an identified, isolated lepton. Signal regions are defined by the number of jets, the number of jets identified as a product of b quark fragmentation (b-tagged jets), the scalar sum of jet transverse momenta (H_T), and M_{T2} . The observed event yields in these regions are compared with the background expectation from standard model (SM) processes and the predicted contributions from simplified supersymmetric models of gluino and squark pair production [21–25].

2 The CMS detector

The central feature of the CMS apparatus is a superconducting solenoid, 13 m in length and 6 m in diameter, which provides an axial magnetic field of 3.8 T. Within the field volume are several particle detection systems. Charged-particle trajectories are measured with silicon pixel and strip trackers, covering $0 \leq \phi < 2\pi$ in azimuth and $|\eta| < 2.5$ in pseudorapidity, where $\eta \equiv -\ln[\tan(\theta/2)]$ and θ is the polar angle of the trajectory of the particle with respect to the beam direction. The transverse momentum, the component of the momentum p in the plane orthogonal to the beam, is defined in terms of the polar angle as $p_T = p \sin \theta$. A lead-tungstate crystal electromagnetic calorimeter and a brass and scintillator hadron calorimeter surround the tracking volume, providing energy measurements of electrons, photons, and hadronic jets in the range $|\eta| < 3.0$. Muons are identified and measured within $|\eta| < 2.4$ by gas-ionization detectors embedded in the steel flux-return yoke of the solenoid. Forward calorimeters on each side of the interaction point encompass $3.0 < |\eta| < 5.0$. The detector is nearly hermetic, allowing momentum imbalance measurements in the plane transverse to the beam direction. A two-tier trigger system selects pp collision events of interest for use in physics analyses. A more detailed description of the CMS detector is available in Ref. [26].

3 Simulated event samples

Monte Carlo (MC) simulations are used in the estimate of some of the SM backgrounds, as well as to calculate the selection efficiency for various new physics scenarios. The main background and control samples (W +jets, Z +jets, $t\bar{t}$ +jets, γ +jets, and QCD multijet events), as well as signal samples of gluino and squark pair production, are generated with the MADGRAPH 5 generator [27] interfaced with PYTHIA 8.2 [28] for fragmentation and parton showering. Signal processes are generated at leading order with up to two extra partons present in the event. Other background samples are generated with MADGRAPH_AMC@NLO 2.2 [29] (s channel single top, $t\bar{t}W$, $t\bar{t}Z$, $t\bar{t}H$) and with POWHEG v2 [30, 31] (t channel single top, tW), both interfaced with PYTHIA 8.2 [28].

Next-to-leading order (NLO) and next-to-NLO cross sections [29–34] are used to normalize the simulated background samples, while NLO plus next-to-leading-logarithm (NLL) calculations [35] are used for the signal samples. The NNPDF3.0LO and NNPDF3.0NLO [36] parton distribution functions (PDF) are used, respectively, with MADGRAPH, and with POWHEG v2 and MADGRAPH_AMC@NLO. Standard model processes are simulated using a GEANT4 based model [37] of the CMS detector, while the simulation of new physics signals is performed using the CMS fast simulation package [38]. All simulated events include the effects of pileup, i.e. multiple pp collisions within the same or neighboring bunch crossings, and are processed with the same chain of reconstruction programs as used for collision data.

4 Event reconstruction

Event reconstruction is based on the particle-flow (PF) algorithm [39, 40], which combines information from the tracker, calorimeter, and muon systems to reconstruct and identify PF candidates, i.e. charged and neutral hadrons, photons, muons, and electrons. We select events with at least one reconstructed vertex that is within 24 cm (2 cm) of the center of the detector in the direction along (perpendicular to) the beam axis. In the presence of pileup, usually more than one such vertex is reconstructed. We designate as the primary vertex (PV) the one for which the summed p_T^2 of the associated charged PF candidates is the largest.

Charged PF candidates associated with the PV and neutral particle candidates are clustered into jets using the anti- k_T algorithm [41] with a distance parameter of 0.4. The jet energy is calibrated using a set of corrections similar to those developed for the 8 TeV data [42]: an offset correction accounting for neutral energy arising from pileup interactions in the area of the reconstructed jet; a relative correction that makes the jet energy response, i.e. the ratio of the reconstructed to the original jet energy, uniform in p_T and η ; an absolute correction that restores the average jet energy response to unity; and a residual correction, applied to account for remaining differences between data and simulation.

Jets originating from b quarks are identified by the combined secondary vertex algorithm [43]. We use a working point with a tagging efficiency of approximately 65% for jets originating from b quarks with momenta typical of top quark pair events. For jets with transverse momentum above approximately 200 GeV, the tagging efficiency decreases roughly linearly, reaching an efficiency of about 45% at 600 GeV. The probability to misidentify jets arising from c quarks as b jets is about 12%, while the corresponding probability for light-flavor quarks or gluons is about 1.5%.

The transverse hadronic energy, H_T , is defined as the scalar sum of the magnitudes of the jet transverse momenta, while the missing transverse hadronic momentum, H_T^{miss} , is defined as

the negative vector sum of the transverse momenta of the same jets. Except for a few cases described later, the construction of higher-level variables and the event categorization are based on jets with $p_T > 30 \text{ GeV}$, $|\eta| < 2.5$, and passing loose requirements on the jet composition designed to reject rare spurious signals arising from noise and failures in the event reconstruction [44]. The transverse momentum imbalance (\vec{p}_T^{miss}), whose magnitude is referred to as E_T^{miss} , is defined as the negative of the vector sum of the transverse momenta of all reconstructed charged and neutral PF candidates.

Electron candidates are reconstructed as clusters of energy deposits in the electromagnetic calorimeter, matched to tracks in the silicon tracker [45]. We identify electrons having $p_T > 10 \text{ GeV}$ by loose requirements on the shape of these energy deposits, on the ratio of energy in associated hadron and electromagnetic calorimeter cells (H/E), on the geometric matching between the energy deposits and the associated track, and on the consistency between the energy reconstructed from calorimeter deposits and the momentum measured in the tracker. In addition, we require that the associated track be consistent with originating from the PV. The PF algorithm applies a looser set of requirements to identify ‘‘PF electrons’’ with even smaller transverse momenta. We use it to extend the range of identified electrons down to $p_T > 5 \text{ GeV}$.

Muon candidates are reconstructed by combining tracks found in the muon system with corresponding tracks in the silicon detectors. Candidates are required to be classified as either *Global Muons* or *Tracker Muons*, according to the definitions given in Ref. [46], when they have $p_T > 10 \text{ GeV}$. The associated silicon detector track is required to be consistent with originating from the PV. The PF algorithm applies looser requirements to identify ‘‘PF muons’’ with even smaller transverse momenta. We use it to extend the range of identified muons down to $p_T > 5 \text{ GeV}$.

The isolation of electrons and muons is defined as the scalar sum of the transverse momenta of all neutral and charged PF candidates within a cone $\Delta R = \sqrt{(\Delta\eta)^2 + (\Delta\phi)^2}$ along the lepton direction. The variable is corrected for the effects of pileup using an effective area correction [47], and the size of the cone is dependent on the lepton p_T according to:

$$\Delta R = \begin{cases} 0.2, & p_T \leq 50 \text{ GeV}, \\ \frac{10 \text{ GeV}}{p_T}, & 50 < p_T \leq 200 \text{ GeV}, \\ 0.05, & p_T > 200 \text{ GeV}. \end{cases} \quad (1)$$

The relative lepton isolation is the lepton isolation divided by the lepton p_T .

When selecting PF electrons and muons, as well as isolated PF charged hadrons, a track-only isolation computed in a larger cone is used. Relative track isolation is calculated using all charged PF candidates within a cone $\Delta R < 0.3$ and longitudinal impact parameter $|\Delta z| < 0.1 \text{ cm}$ relative to the PV.

The efficiency for selecting prompt electrons, i.e., electrons from decays of electroweak bosons or SUSY particles, increases from 65–70% at a p_T of 10 GeV to 80–90% at 50 GeV, and plateaus at 85–95% above 100 GeV, where the smaller values are from signal samples with high jet multiplicity and the larger numbers are from $t\bar{t}$ +jets events. For prompt muons, the efficiency increases from 75–90% at a p_T of 10 GeV to 85–95% at 50 GeV, and plateaus at 95–99% above 200 GeV.

Photon candidates, used in the estimation of the $Z \rightarrow \nu\bar{\nu}$ background, are reconstructed from deposits in the electromagnetic calorimeter and are selected using the shower shape variable

Table 1: The three signal triggers and the corresponding offline selections.

Online trigger selection [GeV]	Offline selection [GeV]
$H_T > 800$	$H_T > 1000 \ \& \ E_T^{\text{miss}} > 30$
$H_T > 350 \ \& \ E_T^{\text{miss}} > 100$	$H_T > 450 \ \& \ E_T^{\text{miss}} > 200$
$H_T^{\text{miss}} > 90 \ \& \ E_T^{\text{miss}} > 90 \ \& \ \text{noise removal criteria}$	$H_T > 200 \ \& \ E_T^{\text{miss}} > 200$

($\sigma_{\eta\eta}$) and the ratio H/E [48]. Additionally, we require that their track isolation in a cone $\Delta R < 0.3$ be less than 2.5 GeV.

5 Event selection

Before assigning events to different signal regions, the baseline selection described in this section is implemented. Collision events are selected using triggers with different requirements on H_T , E_T^{miss} , and H_T^{miss} . Table 1 summarizes the triggers and corresponding offline selections, after which the triggers are found to be $>98\%$ efficient. As shown in the table, events with $H_T < 1000$ GeV are selected with triggers that impose an E_T^{miss} requirement. As a consequence, for the low H_T sample we employ a tighter requirement on the offline value of E_T^{miss} .

The events passing the selections of Table 1 are further divided according to the total number of jets (N_j) and the number of jets identified as originating from b quarks (N_b). When determining N_b , we lower the jet p_T threshold from 30 to 20 GeV in order to increase sensitivity to potential signal scenarios with soft decay products.

For events with at least two reconstructed jets, we start with the pair having the largest dijet invariant mass and iteratively cluster all selected jets using a hemisphere algorithm that minimizes the Lund distance measure [49, 50] until two stable pseudo-jets are obtained. The resulting pseudo-jets together with the \vec{p}_T^{miss} are used to determine the stransverse mass M_{T2} [18, 19]. This kinematic mass variable, which can be considered as a generalization of the transverse mass variable M_T defined in Ref. [51], was introduced as a means to measure the mass of pair-produced particles in situations where both decay to a final state containing the same type of undetected particle. The variable M_{T2} is defined as:

$$M_{T2} = \min_{\vec{p}_T^{\text{miss}X(1)} + \vec{p}_T^{\text{miss}X(2)} = \vec{p}_T^{\text{miss}}} \left[\max \left(M_T^{(1)}, M_T^{(2)} \right) \right], \quad (2)$$

where $\vec{p}_T^{\text{miss}X(i)}$ (with $i = 1, 2$) are the unknown transverse momenta of the two undetected particles and $M_T^{(i)}$ the transverse masses obtained by pairing any of the two invisible particles with one of the two pseudojets. The minimization is performed over trial momenta of the undetected particles fulfilling the \vec{p}_T^{miss} constraint. Most of the background from QCD multijet events (defined more precisely in Section 6) is characterized by very small values of M_{T2} , while a wide class of new physics models imply large values of stransverse mass. Figure 1 shows the M_{T2} distributions expected from simulation for the background processes and one signal model, the gluino-mediated bottom squark production described in Refs. [21–25] and Section 7. Selections based on the M_{T2} variable are a powerful means to reduce the contribution from multijet events to a subleading component of the total background. A complete discussion of the M_{T2} properties as a discovery variable and details about the exact calculation of the variable are given in Refs. [13, 20].

The main selection to suppress the background from multijet production is the requirement $M_{T2} > 200$ GeV in events with at least two reconstructed jets. Even after this requirement,

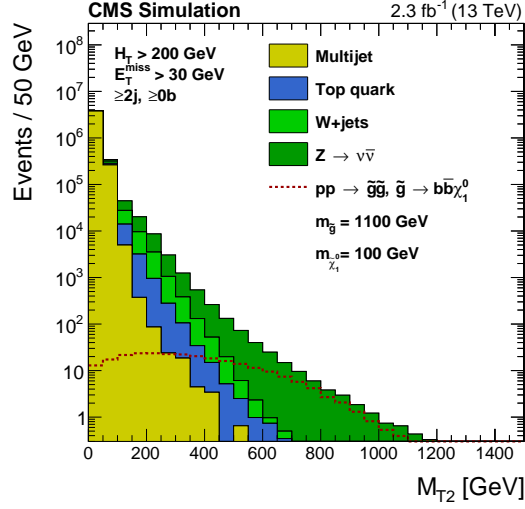


Figure 1: Distribution of the M_{T2} variable in simulated background and signal event samples after the baseline selection is applied. The line shows the expected M_{T2} distribution for a signal model of gluino-mediated bottom squark production with the masses of gluino and lightest neutralino equal to 1100 and 100 GeV, respectively. The simplified signal model is described in Refs. [21–25] and in the text.

a residual background contribution with larger M_{T2} values remains, arising primarily from events in which the energy of a jet has been severely underestimated. To further suppress background events resulting from this effect, we require $\Delta\phi_{\min} > 0.3$, where $\Delta\phi_{\min}$ is defined as minimum azimuthal angle between the \vec{p}_T^{miss} vector and up to four highest p_T jets. For the purpose of the $\Delta\phi_{\min}$ calculation only, we consider jets with $|\eta| < 4.7$. The number and definition of jets entering the $\Delta\phi_{\min}$ calculation are chosen to maximize signal to background separation. In addition, we require that the magnitude of the vector difference in the transverse momentum imbalance determined using either the selected jets (\vec{H}_T^{miss}) or all PF candidates (\vec{p}_T^{miss}) satisfy $|\vec{p}_T^{\text{miss}} - \vec{H}_T^{\text{miss}}|/E_T^{\text{miss}} < 0.5$. This requirement protects against large imbalances arising from objects with $p_T < 30$ GeV or $|\eta| > 2.5$. Finally, events with possible contributions from beam halo processes or anomalous noise in the calorimeters are rejected using dedicated filters [52].

To reduce the background from SM processes with genuine E_T^{miss} arising from the decay of a W boson, we reject events with an identified electron or muon with $p_T > 10$ GeV and $|\eta| < 2.4$. Only electrons (muons) with a relative isolation less than 0.1 (0.2) are considered in the veto. Events are also vetoed if they contain an isolated charged PF candidate (electron, muon or charged hadron) to reject τ leptons decaying to leptons or hadrons. To avoid loss of efficiency in potential signals with large jet multiplicities, events are only vetoed if the transverse mass (M_T) formed by the momentum of the isolated charged PF candidate and \vec{p}_T^{miss} is less than 100 GeV, consistent with the leptonic decay of a W boson. For charged candidates identified as a PF electron or muon, we veto the event if the candidate has $p_T > 5$ GeV and a relative track isolation of less than 0.2. For charged candidates identified as a PF hadron, we veto the event if the candidate has $p_T > 10$ GeV and a relative track isolation of less than 0.1.

5.1 Signal regions

Signal regions are defined separately for events with either exactly one jet passing the counting criteria above, or with two or more jets. Events with $N_j \geq 2$ are categorized based on H_T , N_j , N_b as follows:

- 5 bins in H_T : [200,450], [450, 575], [575, 1000], [1000, 1500], and >1500 . These bins, which are expressed in GeV, are also referred to as very low H_T , low H_T , medium H_T , high H_T , and extreme H_T regions,
- 11 bins in N_j and N_b : 2-3j & 0b, 2-3j & 1b, 2-3j & 2b, 4-6j & 0b, 4-6j & 1b, 4-6j & 2b, $\geq 7j$ & 0b, $\geq 7j$ & 1b, $\geq 7j$ & 2b, 2-6j & $\geq 3b$, $\geq 7j$ & $\geq 3b$.

Each bin defined by the H_T , N_j , N_b requirements above is referred to as a “topological region”.

Since SUSY events could result in M_{T2} distributions harder than the remaining SM backgrounds, we further divide each topological region in bins of M_{T2} , expressed in GeV, as follows:

- 3 bins at very-low H_T : [200,300], [300,400], and >400 ,
- 4 bins at low H_T : [200,300], [300,400], [400,500], and >500 ,
- 5 bins at medium H_T : [200,300], [300,400], [400,600], [600,800], and >800 ,
- 5 bins at high H_T : [200,400], [400,600], [600,800], [800, 1000], and >1000 ,
- 5 bins at extreme H_T : [200,400], [400,600], [600,800], [800,1000], and >1000 .

For events with $N_j = 1$, i.e. belonging to the “monojet” signal regions, the M_{T2} variable is not defined. We instead opt for a simpler strategy with signal regions defined by the p_T of the jet and N_b :

- N_b : 0b, $\geq 1b$,
- 7 bins in jet p_T , indicated in GeV, which are defined as follows: [200,250], [250,350], [350,450], [450,575], [575,700], [700,1000], and >1000 .

In order to have more than one event expected in each signal region, the actual M_{T2} (or jet p_T) binning is coarser than indicated above for some of the topological regions. A complete list of the signal bins is provided in Tables A.1, A.2, and A.3 in Appendix A. In total, we define 172 separate signal regions.

6 Backgrounds

There are three sources of SM background to potential new physics signals in a jets plus E_T^{miss} final state:

- “Lost lepton background”: events with genuine invisible particles, i.e. neutrinos, from leptonic W boson decays where the charged lepton is either out of acceptance, not reconstructed, not identified, or not isolated. This background comes from both W+jets and $t\bar{t}$ +jets events, with a small contribution from single top quark production, and is one of the dominant backgrounds in nearly all search regions. It is estimated using a one-lepton control sample, obtained by inverting the lepton veto in each topological region.
- “Z $\rightarrow \nu\bar{\nu}$ background”: Z+jets events where the Z boson decays to neutrinos. This almost irreducible background is most similar to potential signals. It is a major background in nearly all search regions, its importance decreasing for tighter requirements on N_b . This background is estimated using γ +jets and Z $\rightarrow \ell^+\ell^-$ control samples.
- “Multijet background”: mostly instrumental background that enters a search region because of either significant mismeasurement of the jet momentum or sources of anomalous noise in the detector. There is also a small contribution from events with

genuine E_T^{miss} from neutrinos produced in semi-leptonic decays of charm and bottom quarks. To suppress this background we apply the selections described in Section 5, after which this type of background is sub-dominant in almost all search regions. The background is estimated from a control sample obtained by inverting the $\Delta\phi_{\text{min}}$ requirement in each topological region.

For all three categories, the event yields in the control regions are translated into background estimates in the signal regions using “transfer factors”, either based on simulation or measured in data, which are described in the next sections.

6.1 Estimation of the background from leptonic W boson decays

Single-lepton control regions are used to estimate the background arising from leptonic W boson decays in W +jets and $t\bar{t}$ +jets processes. Control region events are selected using the same triggers as for signal regions, and the baseline selections of Section 5 are applied with the exception of the lepton veto. Instead, we require exactly one lepton candidate passing either the PF lepton selection (e or μ only) or the lepton selection used in lepton vetoes. In addition, we require $M_T(\ell, \vec{p}_T^{\text{miss}}) < 100$ GeV to reduce potential contamination from signal.

Selected events are then grouped into the categories described in Section 5.1, binning the single-lepton control regions in the H_T , N_j , and N_b dimensions, but not in M_{T2} , to preserve statistical precision. The binning in N_j and N_b is the same as that of the signal regions, except for signal bins with $N_j \geq 7$ and $N_b \geq 1$. For these signal regions, the background prediction is obtained using a control region with the same H_T selection as the signal and requiring $N_j \geq 7$ and $1 \leq N_b \leq 2$. This is motivated by the scarcity of data in control regions with $N_j \geq 7$ and $N_b \geq 2$ as well as potential contamination from signal in bins with $N_j \geq 7$ and $N_b \geq 3$. For events with $N_j = 1$, one control region is defined for each bin of jet p_T .

The background yield $N_{1\ell}^{\text{SR}}$ in each signal region SR is obtained from the corresponding single-lepton yield $N_{1\ell}^{\text{CR}}$ in the control region CR by the application of transfer factors $R_{\text{MC}}^{0\ell/1\ell}$ and k_{MC} , and according to the following equation:

$$N_{1\ell}^{\text{SR}}(H_T, N_j, N_b, M_{T2}) = N_{1\ell}^{\text{CR}}(H_T, N_j, N_b) R_{\text{MC}}^{0\ell/1\ell}(H_T, N_j, N_b) k_{\text{MC}}(M_{T2}). \quad (3)$$

The number of events for which we fail to reconstruct or identify an isolated lepton candidate is obtained via the factor $R_{\text{MC}}^{0\ell/1\ell}(H_T, N_j, N_b)$, which accounts for lepton acceptance and selection efficiency and the expected contribution from the decay of W bosons to hadrons through an intermediate τ lepton. The factor $R_{\text{MC}}^{0\ell/1\ell}$ is obtained from simulation and corrected for small measured differences in lepton efficiency between data and simulation. The fraction of events in each topological region expected to populate a particular M_{T2} bin, $k_{\text{MC}}(M_{T2})$, is used to obtain the estimate in each search bin and is also obtained from simulation.

Normalization to data control regions reduces reliance on the MC modeling of most kinematic quantities, except M_{T2} . The uncertainty in $k_{\text{MC}}(M_{T2})$ is evaluated in simulation by variations of the important experimental and theoretical parameters. Reconstruction uncertainties, assessed by varying the tagging efficiency for b quarks, and by evaluating the impact of variations in jet response on the counting of jets and b-tagged jets, E_T^{miss} , and M_{T2} , are typically found to be less than 10%, but can reach as much as 40% in some bins. Renormalization and factorization scales, PDFs [53], and the relative composition of W +jets and $t\bar{t}$ +jets are varied to assess the dominant theoretical uncertainties, which are found to be as large as 30%. Based on these results, for $k_{\text{MC}}(M_{T2})$ we assign a shape uncertainty that reaches 40% in the highest bins of M_{T2} .

The MC modeling of the M_{T2} distribution is checked in data using control regions enriched in events originating from either W +jets or $t\bar{t}$ +jets, as shown in the left and right plots of Fig. 2, respectively. An additional check is performed by comparing the standard estimate with that obtained by replacing the factor $k_{\text{MC}}(M_{T2})$ in Eq. (3), with an extra dimension in the binning of the control region, which becomes $N_{1\ell}^{\text{CR}}(H_T, N_j, N_b, M_{T2})$. The two estimates agree within the statistical precision permitted by the size of the control regions.

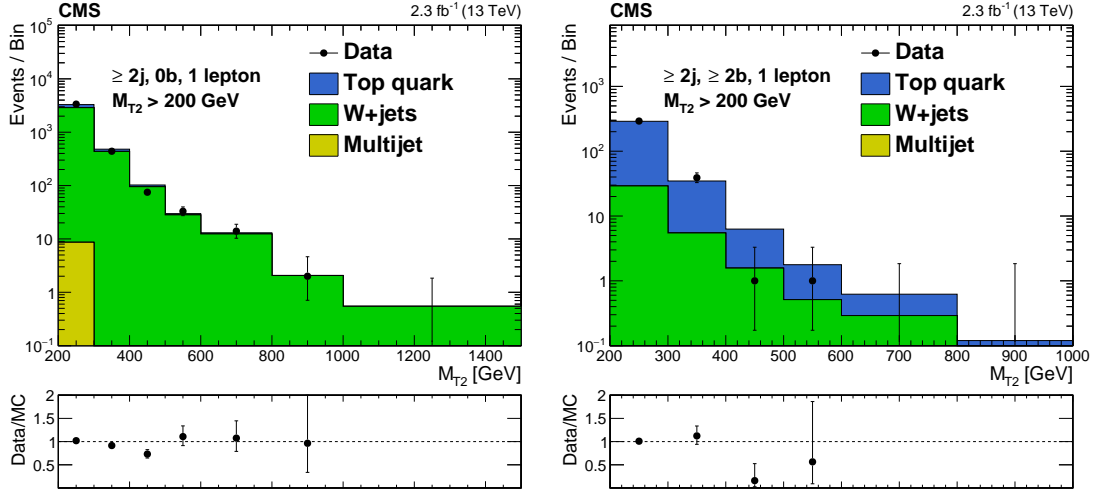


Figure 2: Comparison between simulation and data in the M_{T2} observable. The left and right plots correspond to control samples enriched in W +jets and $t\bar{t}$ +jets, respectively. The sum of the distributions from simulation is scaled to have the same integral as the corresponding histograms from data. The uncertainties shown are statistical only.

The single-lepton control regions typically have 1–2 times as many events expected as compared to the corresponding signal region. The statistical uncertainty in this event yield ranges from 1 to 100%, depending on the region, and is propagated to the final uncertainty in the background estimate. The transfer factor $R_{\text{MC}}^{0\ell/1\ell}$ depends on the MC modeling of the lepton veto and M_T selection efficiencies. Leptonic Z boson decays are used to evaluate the MC modeling of lepton selection efficiencies, and the resulting uncertainty propagated to the background estimate is found to be as large as 7%. The M_T selection efficiency is cross-checked using a similar dilepton sample and removing one of the leptons to mimic events where the W boson decays to a lepton, and an uncertainty of 3% is assigned by comparing data to simulation. The uncertainty in the MC modeling of the lepton acceptance, assessed by varying the renormalization and factorization scales and PDF sets, is found to be as large as 5%. Finally, the uncertainty in the b tagging efficiency and the jet energy scale is typically less than 10%, although it can be as large as 40% in some bins.

The effect of signal contributions to the lost-lepton control samples can be non negligible in some parts of signal parameter space, and is taken into account in the interpretations presented in Section 7. Such a contribution would cause an overestimate of the lost-lepton background in the signal regions. In order to account for this effect, which is typically small but can become as large as 20% in some compressed scenarios, the predicted signal yield in each signal region is corrected by the amount by which the background would be overestimated.

6.2 Estimation of the background from $Z(\nu\bar{\nu})+\text{jets}$

The $Z \rightarrow \nu\bar{\nu}$ background is estimated using a $\gamma+\text{jets}$ control sample selected using a single-photon trigger. We select events where the photon has $p_T > 180$ GeV, to mimic the implicit requirement on the p_T of the Z boson arising from the baseline selection $M_{T2} > 200$ GeV, and $|\eta| < 2.5$. The full baseline selection requirements are made based on kinematic variables re-calculated after removing the photon from the event, to replicate the $Z \rightarrow \nu\bar{\nu}$ kinematics.

Adopting a similar strategy as that used for the estimation of the lost-lepton background, selected events are then grouped into the categories described in Section 5.1, binning the photon control regions in the H_T , N_j , and N_b dimensions, but not in M_{T2} , to preserve statistical precision. For events with $N_j = 1$, one control region is defined for each bin of jet p_T . The background estimate $N_{Z \rightarrow \nu\bar{\nu}}^{\text{SR}}$ in each signal bin is obtained from the events yield N_γ^{CR} in the control region by the application of transfer factors according to Eq. (4):

$$N_{Z \rightarrow \nu\bar{\nu}}^{\text{SR}}(H_T, N_j, N_b, M_{T2}) = N_\gamma^{\text{CR}}(H_T, N_j, N_b) P_\gamma(H_T, N_j, N_b) f R_{\text{MC}}^{Z/\gamma}(H_T, N_j, N_b) k_{\text{MC}}(M_{T2}). \quad (4)$$

The prompt-photon purity, P_γ , which accounts for photons arising from meson decays, is measured in data by performing a template fit of the charged-hadron isolation distribution for each H_T , N_j , and N_b region. The shape of the template for prompt photons is obtained from data by measuring the charged-hadron activity in cones well-separated from the photon and any jet. The isolation template for background photons arising from meson decays, which happen normally within hadronic jets, is also obtained from data using photon candidates that fail the $\sigma_{\eta\eta}$ requirement. A prompt photon purity of 90–100%, as measured in data, is well reproduced by simulation as seen in the left plot of Fig. 3. A separate determination of the prompt photon purity using a tight-to-loose ratio method [54] obtained from the charged-hadron isolation sideband is found to yield consistent results.

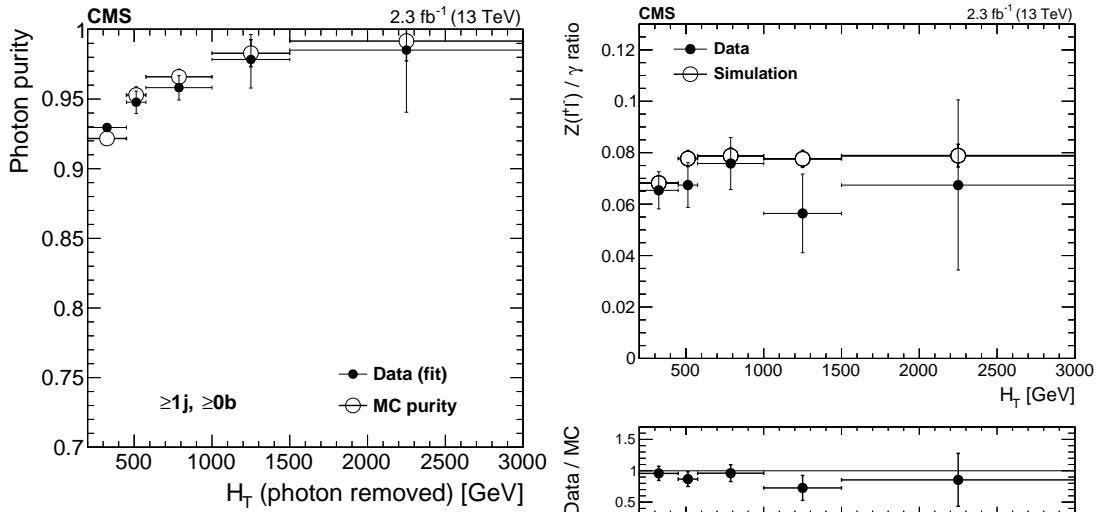


Figure 3: The left plot shows the photon purity, P_γ , measured in data for the single-photon control sample compared with the values extracted from simulation. The right plots show the Z/γ ratio in simulation and data as a function of H_T (upper plot), and the corresponding double ratio (lower plot).

The $Z \rightarrow \nu\bar{\nu}$ background in each bin of H_T , N_j , and N_b is obtained from the corresponding pho-

ton control region yield via the factor $R_{\text{MC}}^{Z/\gamma}$, which accounts for the photon acceptance and selection efficiency and the ratio of cross sections for the production of Z+jets and γ +jets events.

The ratio $R_{\text{MC}}^{Z/\gamma}$ is obtained from γ +jet events simulated with MADGRAPH with an implicit requirement $\Delta R > 0.4$ between the prompt photon and the nearest parton. As no such requirement can be made in data, a correction factor $f = 0.92$ is applied to account for the fraction of selected photons passing the ΔR requirement. This factor is determined from studies with samples of MADGRAPH+PYTHIA and PYTHIA-only multijet events, the latter having no explicit requirement on the separation between the photon and the nearest parton. The ratio $R_{\text{MC}}^{Z/\gamma}$ obtained from simulation is validated in data using $Z \rightarrow \ell^+\ell^-$ events. In this validation, the baseline selection is applied to the $Z \rightarrow \ell^+\ell^-$ sample after removing the reconstructed leptons from the event, to replicate the kinematics of $Z \rightarrow \nu\bar{\nu}$, and the top-quark background contamination is subtracted. The upper right plot of Fig. 3 shows the $R^{Z/\gamma}$ ratios in simulation and in data, while the double ratio, $R_{\text{data}}^{Z \rightarrow \ell^+\ell^-/\gamma} / R_{\text{MC}}^{Z \rightarrow \ell^+\ell^-/\gamma}$, is shown in the lower right plot. The values are shown in bins of H_T , after corrections to account for measured differences between data and simulation in lepton and photon selection efficiencies and in b tagging. The double ratio shows no significant trend as a function of H_T , and a correction factor of 0.95 is applied to $R_{\text{MC}}^{Z/\gamma}$ to account for the observed deviation from unity. Similarly, the double ratio as a function of N_j and N_b shows no significant trends and is found to be consistent with unity after the same correction factor is applied.

As in the case of the estimate of the single-lepton background, normalization to data control regions reduces reliance on the MC modeling to a single dimension, M_{T2} . The fraction of events in each topological region expected to populate a particular M_{T2} bin, $k_{\text{MC}}(M_{T2})$, is used to obtain the estimate in each search bin. The uncertainty in this fraction in each M_{T2} bin is evaluated in simulation by variations of the important experimental and theoretical quantities. Theoretical uncertainties represent the largest contribution, and are assessed by variations of the renormalization and factorization scales and PDF sets. Smaller contributions from reconstruction uncertainties are determined by varying the b-tagging efficiency and the mistag rate, and by evaluating the impact of variations in jet energy response on the counting of jets and b-tagged jets, E_T^{miss} , and M_{T2} . Experimental and theoretical uncertainties in $k_{\text{MC}}(M_{T2})$ total as much as 30% at large values of M_{T2} . Based on these results, we assign an uncertainty for $k_{\text{MC}}(M_{T2})$ that reaches 40% in the highest bins of M_{T2} .

The MC modeling of the M_{T2} variable is checked in data using highly populated control samples of γ +jets and $W \rightarrow \ell\nu$ events. Figure 4 shows good agreement between the M_{T2} distribution obtained from these samples with that from $Z \rightarrow \nu\bar{\nu}$ simulation in the medium- and high- H_T regions. In this comparison, the γ +jets sample is corrected based on P_γ , f , and $R_{\text{MC}}^{Z/\gamma}$, while the W boson sample is corrected for top quark background contamination and rescaled by a $R_{\text{MC}}^{Z/W}$ factor analogous to $R_{\text{MC}}^{Z/\gamma}$. Similarly to what is done for the lost-lepton background, an additional check is performed by comparing the standard estimate with that obtained by replacing the factor $k_{\text{MC}}(M_{T2})$ in Eq. (4) with an extra dimension in the binning of the control region, which becomes $N_\gamma^{\text{CR}}(H_T, N_j, N_b, M_{T2})$. These two estimates agree within the statistical precision permitted by the size of the control regions.

The single-photon control regions typically have 2–3 times as many events as compared to the corresponding signal regions. The statistical uncertainty in this yield ranges from 1 to 100%, depending on the region, and is propagated in the final estimate. The dominant uncertainty in the MC modeling of $R_{\text{MC}}^{Z/\gamma}$ comes from the validation of the ratio using $Z \rightarrow \ell^+\ell^-$ events. One-dimensional projections of the double ratio are constructed—separately in bins of number of

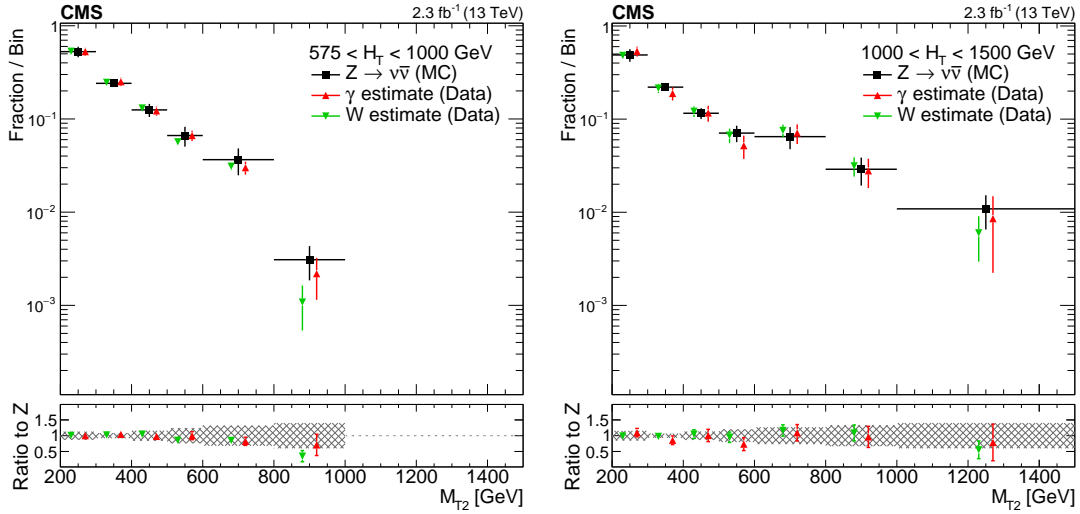


Figure 4: The shape of the M_{T2} distribution from $Z \rightarrow \nu\bar{\nu}$ simulation compared to shapes extracted from γ and W data control samples in the medium- (left plot) and high- H_T regions (right plot). The M_{T2} distributions in the data control samples are obtained after removing the reconstructed γ or lepton from the event, to replicate the kinematics of $Z \rightarrow \nu\bar{\nu}$. The ratio of the shapes derived from data to the $Z \rightarrow \nu\bar{\nu}$ simulation shape is shown in the lower plots, where the shaded band represents the uncertainty in the MC modeling of the M_{T2} variable. Data points are shifted horizontally by ± 20 GeV to make the vertical error bars more visible.

jets, number of b -tagged jets, and H_T (Fig. 3, right)—and an uncertainty in $R_{MC}^{Z/\gamma}$ in each bin of N_j , N_b , and H_T is determined by adding in quadrature the uncertainty in the ratio $R^{Z \rightarrow \ell\ell/\gamma}$ from the corresponding bins of the one-dimensional projections. As sufficient data are not available to evaluate the double ratio for regions with $N_b \geq 3$, and as no trends are visible in the N_b distribution for $N_b < 3$, we assign twice the uncertainty obtained in the nearest bin, i.e. $N_b = 2$. This uncertainty ranges from 10 to 100%, depending on the search region. An additional 11% uncertainty in the transfer factor, based on the observed offset of the double ratio from unity, is added in quadrature with the above.

The uncertainty in the measurement of the prompt photon purity includes a statistical contribution from yields in the isolation sideband that is typically 5–10%, but can reach as much as 100% for search regions requiring extreme values of H_T or large N_j . An additional 5% uncertainty is derived from variations in purity caused by modifications of the signal and background templates, and from a “closure test” of the method in simulation. We indicate with closure test a measurement of the ability of the method to predict correctly the true number of background events when applied to simulated samples. Finally, an uncertainty of 8% is assigned to cover differences in the correction fraction f observed between MADGRAPH+PYTHIA and PYTHIA-only simulations.

6.3 Estimation of the multijet background

The multijet background consists predominantly of light-flavor and gluon multijet events. Though this background is expected to be small after requiring $M_{T2} > 200$ GeV, we estimate any residual contribution based on data control samples. For events with at least two jets, a multijet-enriched control region is obtained in each H_T bin by inverting the $\Delta\phi_{\min}$ requirement described in Section 5. For the high- and extreme- H_T bins, control region events are selected using the same trigger as for signal events. For lower- H_T regions, the online E_T^{miss} requirement precludes the use of the signal trigger, and the control sample is instead selected using

prescaled H_T triggers with lower thresholds. Prescaled triggers accept only a fixed fraction of the events that satisfy their selection criteria.

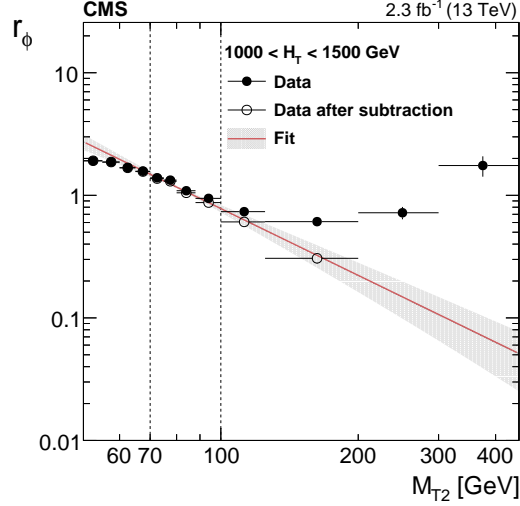


Figure 5: Distribution of the ratio r_ϕ as a function of M_{T2} for the high- H_T region. The fit is performed on the background-subtracted data points (open markers) in the interval $70 < M_{T2} < 100$ GeV delimited by the two vertical dashed lines. The solid points represent the data before subtracting non-multijet backgrounds using simulation. Data point uncertainties are statistical only. The line and the band around it show the fit to a power-law function and the associated uncertainty.

The extrapolation from low- to high- $\Delta\phi_{\min}$ is based on the following ratio:

$$r_\phi(M_{T2}) = N(\Delta\phi_{\min} > 0.3) / N(\Delta\phi_{\min} < 0.3). \quad (5)$$

Studies in simulation show the ratio to be well described by a power law function, $a(M_{T2})^b$. The parameters a, b are determined in each H_T bin by fitting the ratio $r_\phi(M_{T2})$ in a sideband in data, i.e. $60 < M_{T2} < 100$ GeV, after subtracting non-multijet contributions using simulation. For the high- and extreme- H_T regions, the fit is performed in a slightly narrower M_{T2} window, with the lower edge increased to 70 GeV. Data with lower values of M_{T2} are not used, since in these events the E_T^{miss} no longer arises predominantly from underestimated jet energies, but also receives important contributions from the measurement of energy not clustered into jets. The high- M_{T2} boundary of the fitting region is chosen to minimize the effect of the non-multijet contributions mentioned above. An example in the high- H_T region is shown in Fig. 5. The inclusive multijet contribution in each H_T region, $N_{\text{inc}}^{\text{SR}}(M_{T2})$, is estimated using the fitted $r_\phi(M_{T2})$ and the number of events in the low- $\Delta\phi_{\min}$ control region, $N_{\text{inc}}^{\text{CR}}(H_T)$:

$$N_{\text{inc}}^{\text{SR}}(M_{T2}) = N_{\text{inc}}^{\text{CR}}(H_T) r_\phi(M_{T2}). \quad (6)$$

From the inclusive multijet estimate in each H_T region, the predicted background in bins of N_j and N_b is obtained from the following equation

$$N_{j,b}^{\text{SR}}(M_{T2}) = N_{\text{inc}}^{\text{SR}}(M_{T2}) f_j(H_T) r_b(N_j), \quad (7)$$

where f_j is the fraction of multijet events falling in bin N_j , and r_b is the fraction of all events in bin N_j that fall in bin N_b . Simulation indicates that f_j and r_b attain similar values in low- and

high- $\Delta\phi_{\min}$ regions, and that the values are independent of M_{T2} . We take advantage of this to measure the values of f_j and r_b using events with M_{T2} between 100–200 GeV in the low- $\Delta\phi_{\min}$ sideband, where f_j is measured separately in each H_T bin, while r_b is measured in bins of N_j , integrated over H_T , as r_b is found to be independent of the latter. Values of f_j and r_b measured in data are shown in Fig. 6 compared to simulation.

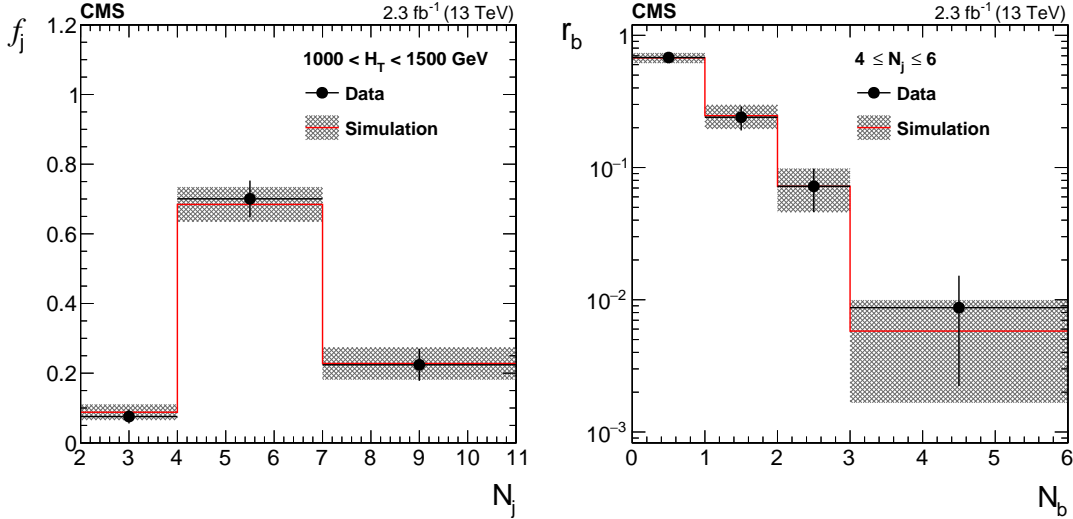


Figure 6: Fraction f_j of multijet events falling in bins of number of jets N_j (left) and fraction r_b of events falling in bins of number of b-tagged jets N_b (right). Values of f_j and r_b are measured in data, after requiring $\Delta\phi_{\min} < 0.3$ and $100 < M_{T2} < 200$ GeV. The bands represent both statistical and systematic uncertainties of the estimate from simulation.

An estimate based on $r_\phi(M_{T2})$ is not viable in the monojet search region so a different strategy must be employed. Multijet events can pass the monojet event selections through rare fluctuations in dijet events, as when the transverse momentum of one of the two jets is severely underestimated because of detector response or because of particularly energetic neutrinos from b and c quark decays. In these cases, the resulting reconstructed jet can be assigned a transverse momentum below the jet-counting threshold ($p_T < 30$ GeV). In order to estimate this background contribution, we define a control region by selecting dijet events in which the leading jet has a transverse momentum $p_T > 200$ GeV (as in the monojet signal region), and the second jet has a transverse momentum just above threshold, i.e. $30 < p_T < 60$ GeV. These events must further pass an inverted $\Delta\phi_{\min}$ requirement, in order to ensure statistical independence from the signal region. After subtracting non-multijet contributions, the data yield in the control region is taken as an estimate of the background in the monojet search regions. The rate of events with $30 < p_T < 60$ GeV is expected to be larger than that of events with $p_T < 30$ GeV, as the latter would require even larger detector response fluctuations. Closure tests on the simulation indicate a small overestimate. Nevertheless, the multijet background is not expected to exceed 8% in any monojet search region.

Statistical uncertainties due to the event yields in the control regions, where the $r_\phi(M_{T2})$ fit is performed and the f_j and r_b values are measured, are propagated to the final estimate. The invariance of f_j with M_{T2} and r_b with M_{T2} and H_T is evaluated in simulation, and residual differences are taken as additional systematic uncertainties, which are shown in Fig. 6. An additional uncertainty is assigned to cover the sensitivity of the r_ϕ value to variations in the fit window. These variations result in an uncertainty that increases with M_{T2} and ranges from 15 to 200%. The total uncertainty in the estimate covers the differences observed in closure tests based on simulation and in data control regions. The latter is performed in the $100 < M_{T2} <$

200 GeV sideband. For the monojet regions, the statistical uncertainty from the data yield in the dijet sideband is combined with a 50% systematic uncertainty in all bins.

6.4 Cross-check of multijet background estimation

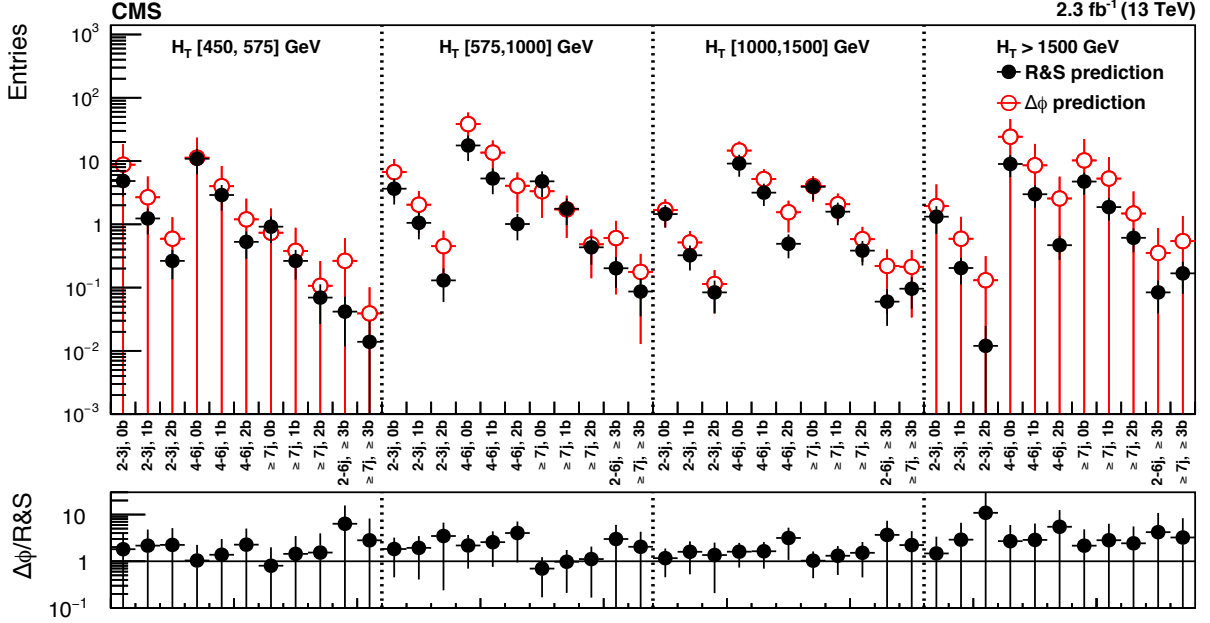


Figure 7: Comparison of the predictions of the multijet background in the topological regions ($M_{T2} > 200$ GeV) from the R&S method and the $\Delta\phi_{\min}$ ratio method. Both methods are described in Ref. [55] and in the text, respectively. The uncertainties are combined statistical and systematic. Within each of the four H_T categories, the estimates from the $\Delta\phi_{\min}$ ratio method are correlated as they are derived from the same fit to the $\Delta\phi_{\min}$ ratio data. The lower plot shows the ratio of the estimates from the $\Delta\phi_{\min}$ and the R&S methods.

As a cross-check of the $\Delta\phi_{\min}$ ratio method described in Section 6.3, the multijet background is also estimated using the “rebalance and smear” (R&S) method described in Ref. [55]. This method rebalances multijet events in data by adjusting the jet p_T values to minimize E_T^{miss} and then smears them multiple times in order to build a large sample of multijet events with nonzero E_T^{miss} . During both the rebalance and the smearing steps, the jet p_T values are varied according to a parameterization of the jet energy response. The performance of the method has been tested on multijet simulation, as well as on data control regions defined by inverting the $\Delta\phi_{\min}$ requirement or by selecting a sideband of M_{T2} (i.e. $100 < M_{T2} < 200$ GeV). Based on these studies, we assign total systematic uncertainties of 50% (low- and medium- H_T regions) and 40% (high- and extreme- H_T regions) in the background estimate based on R&S for $M_{T2} > 200$ GeV. These uncertainties also include a small ($< 7\%$) uncertainty due to contamination from W+jets and Z+jets events of the multijet data sample used in the R&S procedure.

In Fig. 7, we compare the multijet predictions from the R&S method with those from the $\Delta\phi_{\min}$ ratio method, i.e. the estimation method used in our analysis for multijet signal regions. This comparison is done separately for each topological region, integrating over M_{T2} bins. The level of agreement between the two methods serves to further increase our confidence in the multijet background estimation used for the final results of the analysis.

The R&S method cannot be applied to the very-low- H_T region as not enough data are available in the relevant multijet control sample because of the small fraction of events accepted by the prescaled triggers with very low thresholds in H_T .

7 Results and interpretation

Figure 8 shows a summary of the observed event yields in data, together with the predicted total SM background. Each bin in the upper plot corresponds to a single (H_T, N_j, N_b) search region integrated over M_{T2} . The lower plot further breaks down the background estimates and observed data yields into all M_{T2} bins for the medium H_T region. The data are statistically compatible with the expected background contributions, providing no evidence for new physics: analyzing the 87 signal regions with a non-zero excess in the observed data, we see that three bins correspond to a p-value [56] approximately equal to 2σ , zero have a p-value larger than 3σ , and in general all p-values are compatible with a standard normal distribution. The background estimates and corresponding uncertainties shown in these plots rely exclusively on the inputs from control samples and simulation as described in Section 6 and are indicated in the rest of the text as “pre-fit background” results.

We also estimate the backgrounds in the signal regions performing a maximum-likelihood fit to the data in the signal regions themselves. These fits are carried out under either the background-only or background+signal hypotheses. The estimates from these fits, which still depend on the modeling of the backgrounds from the pre-fit procedure, are indicated as “post-fit” results and are utilized to constrain models of new physics as described below. Similar comparisons between data and background predictions, for both pre- and post-fit estimates, are shown for all the remaining H_T regions in Appendix A.

The results of the search are used to constrain specific models [21–25] of new physics such as those identified by the diagrams in Fig. 9. For each scenario of gluino (squark) pair production, our simplified models assume that all supersymmetric particles other than the gluino (squark) and the lightest neutralino are too heavy to be produced directly, and that the gluino (squark) decays promptly. For gluino pair production, the models assume that each gluino decays with a 100% branching fraction into the lightest supersymmetric particle (LSP) and either b quark pairs ($\tilde{g} \rightarrow b\bar{b}\tilde{\chi}_1^0$), top quark pairs ($\tilde{g} \rightarrow t\bar{t}\tilde{\chi}_1^0$), or light-flavor quarks ($\tilde{g} \rightarrow q\bar{q}\tilde{\chi}_1^0$), proceeding respectively through an off-shell bottom, top, or light-flavor squark.

For the scenario of top squark pair production, the polarization of the top quark is model dependent and is a function of the top-squark and neutralino mixing matrices. To remain agnostic to a particular model realization, events are generated without polarization. Also, for the region where $m_{\tilde{t}} - m_{\text{LSP}} < m_t$, a uniform phase-space decay is assumed.

For a given signal scenario, limits are derived by combining all search regions using a modified frequentist approach, employing the CL_s criterion and an asymptotic formulation [57–60].

Typical values of the uncertainties considered in the signal yield for one of the models are listed in Table 2. The largest uncertainties come from the limited size of the MC samples for a small number of model points with low acceptance, and the uncertainty in the b tagging efficiency. The uncertainty in the modeling of initial-state radiation (ISR) can also be significant for model points with small mass splittings, where some boost from ISR is necessary to observe the decay products of the initially produced sparticles. The uncertainty is determined by comparing the simulated and measured p_T spectra of the system recoiling against the ISR jets in $t\bar{t}$ events, using the technique described in Ref. [61]. The two spectra are observed to agree below 400 GeV, and the statistical precision of the comparison is used to define an uncertainty of 15% (30%) for $400 < p_T < 600$ GeV ($p_T > 600$ GeV). The uncertainty in the acceptance due to the renormalization and factorization scales is found to be relatively small, and a constant value of 5% is used in the analysis.

The uncertainty due to the jet energy scale is found to be compatible with statistical fluctuations

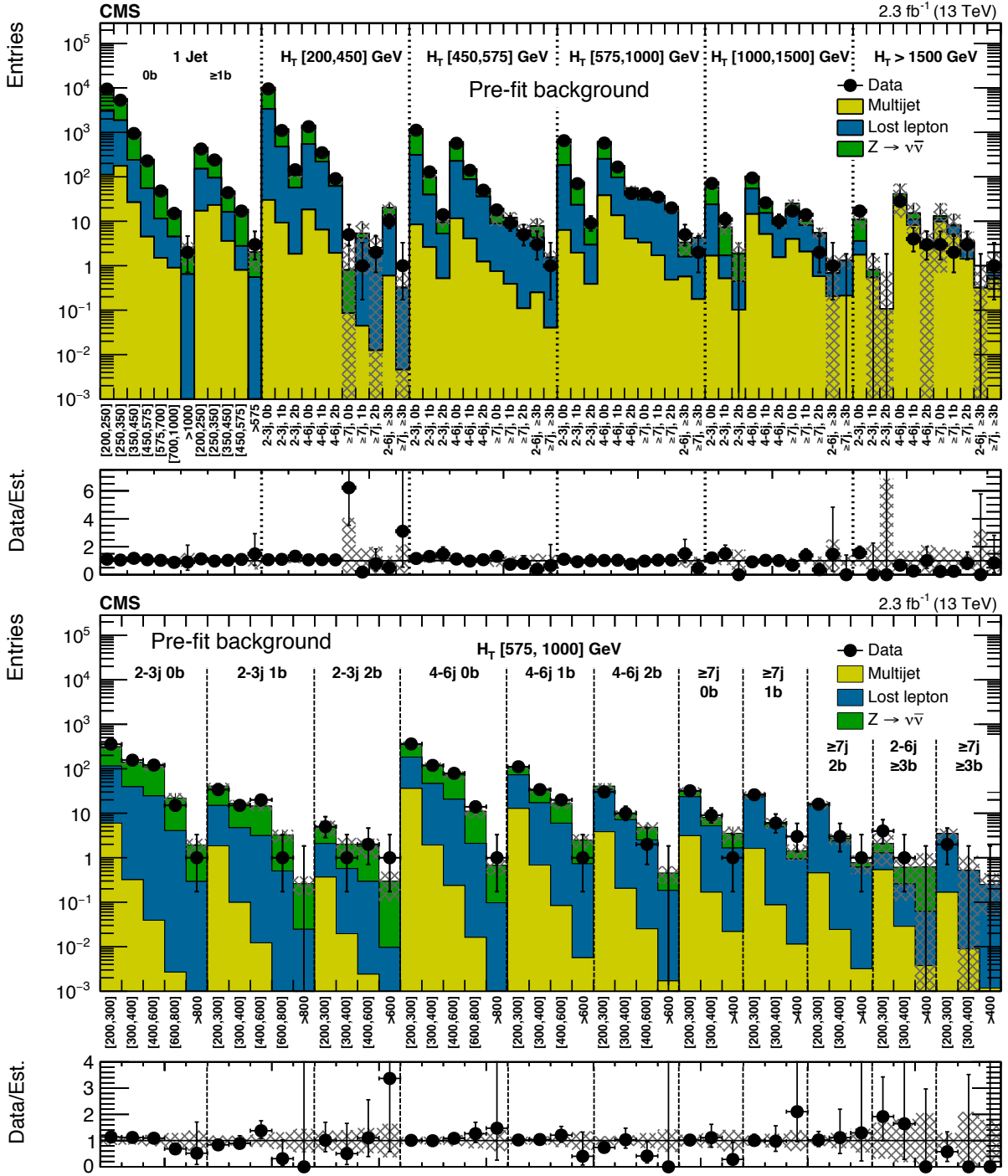


Figure 8: (Above) Comparison of estimated background (pre-fit) and observed data events in each topological region. The results shown for $N_j = 1$ correspond to the monojet search regions binned in jet p_T in GeV. For the multijet data, the notations j and b indicate the N_j and N_b multiplicity. Hatched bands represent the full uncertainty in the background estimate. (Below) Comparison for individual M_{T2} signal bins in the medium H_T region. On the x -axis, the M_{T2} range of each signal region is shown in GeV. Bins with no entry for data have an observed count of 0 events.

for bins populated by few MC events, so a constant value of 5% is taken, motivated by more populated search bins. Uncertainties in the integrated luminosity, ISR, b tagging, and lepton

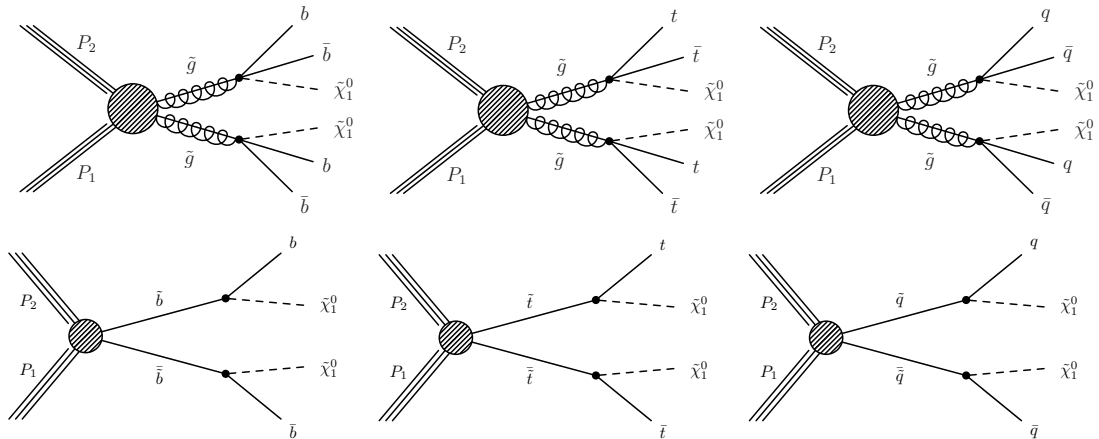


Figure 9: (Above) Diagrams for the three considered scenarios of gluino-mediated bottom squark, top squark, and light flavor squark production. The depicted three-body decays are assumed to proceed through off-shell squarks. (Below) Diagrams for the three considered simplified models of direct pair production of bottom squarks, top squarks, and light flavor squarks. The top quarks in these processes are assumed to be produced unpolarized.

efficiencies are treated as correlated across search bins. No additional uncertainty due to variations of the PDF set is taken since the main effect on signal acceptance is through modeling of the recoil p_T spectrum and the ISR uncertainty already accounts for this.

Figure 10 shows exclusion limits at 95% confidence level (CL) for gluino-mediated bottom squark, top squark, and light-flavor squark production. Exclusion limits for the pair production of bottom, top and light-flavor squarks are shown in Fig. 11. In the upper right plot of this figure, the white diagonal band corresponds to the region $|m_{\tilde{t}} - m_t - m_{\text{LSP}}| < 25 \text{ GeV}$, where the selection efficiency of top squark events is a strong function of $m_{\tilde{t}} - m_{\text{LSP}}$. As a result, the precise determination of the cross section upper limit is uncertain because of the finite granularity of the available MC samples in this region of the $(m_{\tilde{t}}, m_{\text{LSP}})$ plane.

All mass limits shown are obtained using signal cross sections calculated at NLO+NLL order in α_s [62–66]. Table 3 summarizes the limits of the supersymmetric particles excluded in the simplified model scenarios considered.

Table 2: Ranges of typical values of the signal systematic uncertainties as evaluated for the $\tilde{g} \rightarrow b\bar{b}\tilde{\chi}_1^0$ signal model. Uncertainties evaluated on other signal models are consistent with these ranges of values. A large uncertainty from the limited size of the simulated sample only occurs for a small number of model points for which a small subset of search regions have very low efficiency.

Source	Typical values [%]
Integrated luminosity	5
Limited size of MC samples	1–100
Renormalization and factorization scales	5
ISR	0–30
b tagging efficiency, heavy flavor	0–40
b tagging efficiency, light flavor	0–20
Lepton efficiency	0–20
Jet energy scale	5

To facilitate reinterpretation of our results in the context of other models, we have also provided

Table 3: Summary of 95% CL observed exclusion limits for different SUSY simplified model scenarios. The limit on the mass of the produced sparticle is quoted for a massless LSP, while for the lightest neutralino the best limit on its mass is quoted.

Simplified model	Limit on produced sparticle mass [GeV] for $m_{\tilde{\chi}_1^0} = 0$ GeV	Best limit on LSP mass [GeV]
Direct squark production		
Bottom squark	880	380
Top squark	800	300
Single light squark	600	300
8 degenerate light squarks	1260	580
Gluino mediated production		
$\tilde{g} \rightarrow b\bar{b}\tilde{\chi}_1^0$	1750	1125
$\tilde{g} \rightarrow t\bar{t}\tilde{\chi}_1^0$	1550	825
$\tilde{g} \rightarrow q\bar{q}\tilde{\chi}_1^0$	1725	850

predictions and results in “aggregated regions,” made from summing up our individual signal bins in topologically similar regions. These results are presented in Appendix B.

8 Summary

A search for new physics using events containing hadronic jets with transverse momentum imbalance as measured by the M_{T2} variable has been presented. Results are based on a data sample of proton-proton collisions at $\sqrt{s} = 13$ TeV collected with the CMS detector and corresponding to an integrated luminosity of 2.3 fb^{-1} . No significant deviations from the standard model expectations are observed.

In the limit of a massless LSP, gluino masses of up to 1750 GeV are excluded, extending the reach of Run 1 searches by more than 300 GeV. For lighter gluinos, LSP masses up to 1125 GeV in the most favorable models are excluded, also increasing previous limits by more than 300 GeV. Among the three gluino decays considered, the strongest limits on gluino pair production are generally achieved for the $\tilde{g} \rightarrow b\bar{b}\tilde{\chi}_1^0$ channel. Improved sensitivity is obtained in this scenario as selections requiring at least two b-tagged jets in the final state retain a significant fraction of gluino-mediated bottom squark events, while strongly suppressing the background from W+jets, Z+jets, and multijet processes. Also, unlike for models with $\tilde{g} \rightarrow t\bar{t}\tilde{\chi}_1^0$ decays, which include leptonic decays, gluino-mediated bottom squark events do not suffer from an efficiency loss due to the lepton veto.

For direct pair production of first- and second-generation squarks, each assumed to decay exclusively to a quark of the same flavor and the lightest neutralino, squark masses of up to about 1260 GeV and LSP masses up to 580 GeV are excluded. If only a single squark is assumed to be light, the limit on the squark and LSP masses is relaxed to 600 and 300 GeV, respectively. For the pair production of third-generation squarks, each assumed to decay with 100% branching fraction to a quark of the same flavor and the lightest neutralino, a bottom (top) squark mass up to 880 (800) GeV is excluded.

For gluino-induced and direct squark production models, the observed exclusion limits on the masses of the sparticles are from 200 to about 300 GeV higher than those obtained by a similar analysis performed on 8 TeV data [13], which is therefore superseded by the current search. In

relative terms, the largest difference is in the limit on the mass of the top squark, which moves from about 500 GeV to 800 GeV for a massless LSP. This is mostly due to a fluctuation in the 8 TeV data that is not present in the 13 TeV data.

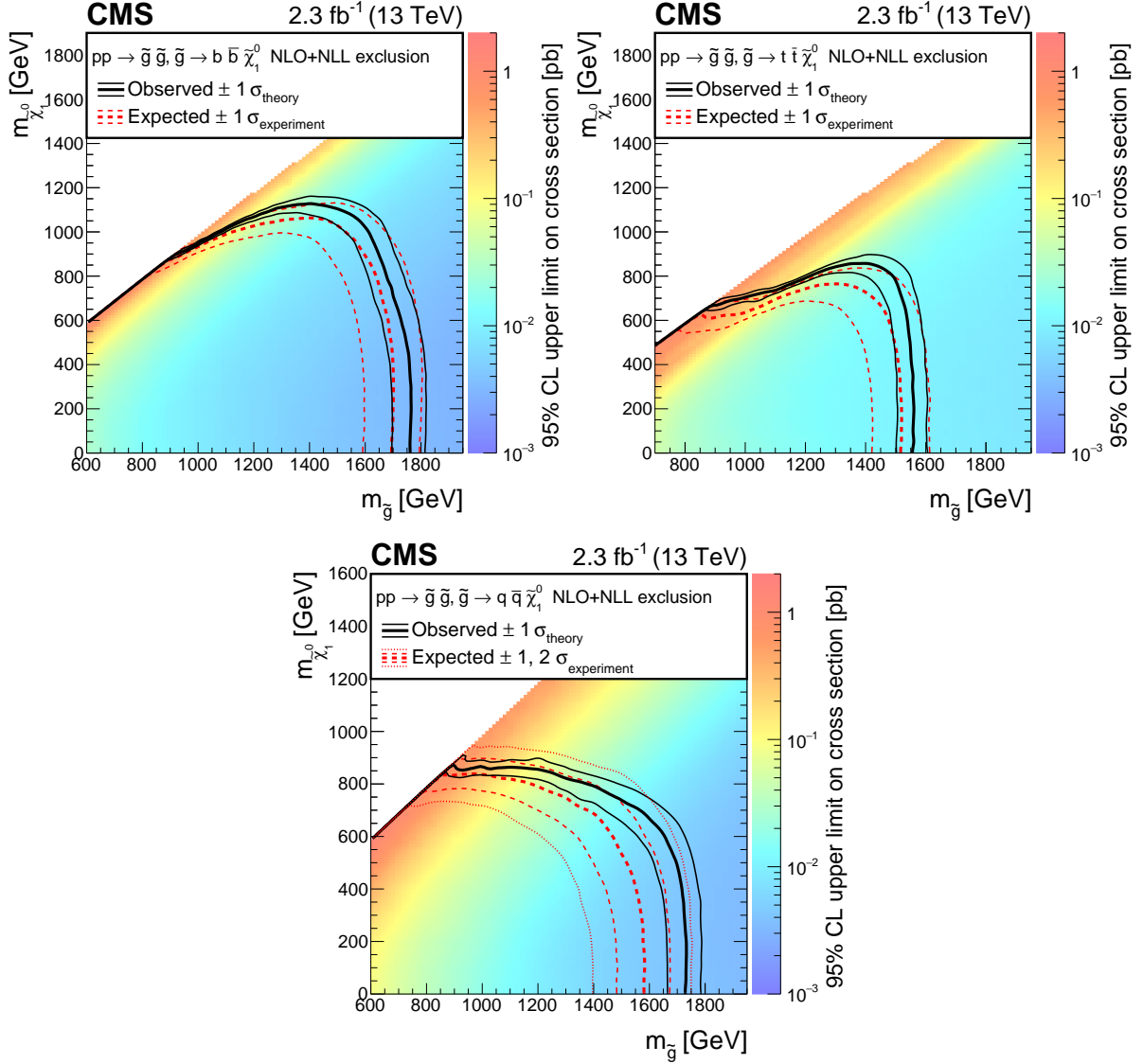


Figure 10: Exclusion limits at 95% CL on the cross sections for gluino-mediated bottom squark production (above left), gluino-mediated top squark production (above right), and gluino-mediated light-flavor squark production (below). The area to the left of and below the thick black curve represents the observed exclusion region, while the dashed red lines indicate the expected limits and their $\pm 1 \sigma_{\text{experiment}}$ standard deviation uncertainties. For the gluino-mediated light-flavor squark production plot, the ± 2 standard deviation uncertainties are also shown. The thin black lines show the effect of the theoretical uncertainties σ_{theory} on the signal cross section.

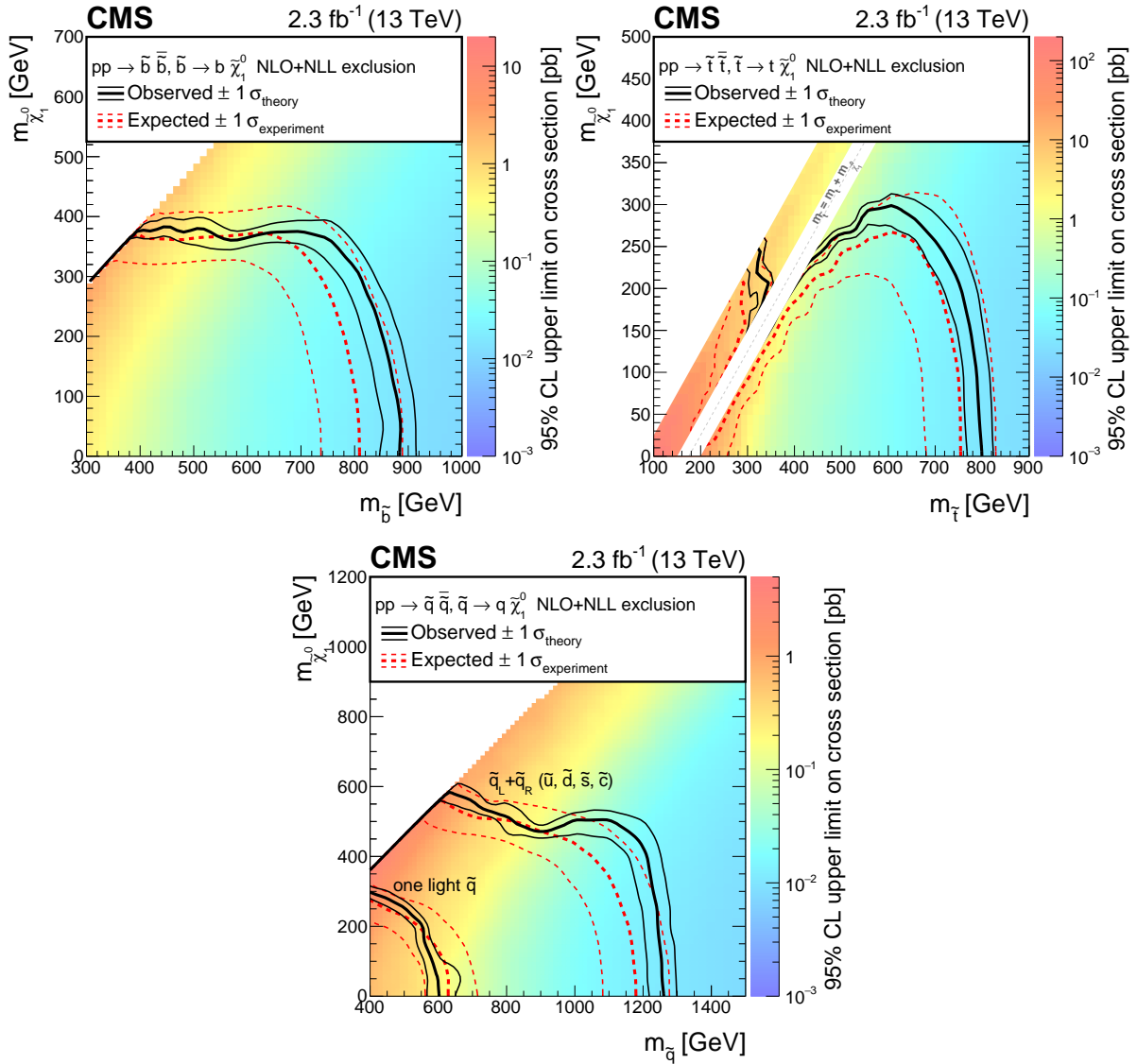


Figure 11: Exclusion limit at 95% CL on the cross sections for bottom squark pair production (above left), top squark pair production (above right), and light-flavor squark pair production (below). The area to the left of and below the thick black curve represents the observed exclusion region, while the dashed red lines indicate the expected limits and their $\pm 1\sigma_{\text{experiment}}$ standard deviation uncertainties. The thin black lines show the effect of the theoretical uncertainties σ_{theory} on the signal cross section. The white diagonal band in the upper right plot corresponds to the region $|m_{\tilde{t}} - m_t - m_{\text{LSP}}| < 25$ GeV. Here the efficiency of the selection is a strong function of $m_{\tilde{t}} - m_{\text{LSP}}$, and as a result the precise determination of the cross section upper limit is uncertain because of the finite granularity of the available MC samples in this region of the $(m_{\tilde{t}}, m_{\text{LSP}})$ plane.

Acknowledgments

We congratulate our colleagues in the CERN accelerator departments for the excellent performance of the LHC and thank the technical and administrative staffs at CERN and at other CMS institutes for their contributions to the success of the CMS effort. In addition, we gratefully acknowledge the computing centers and personnel of the Worldwide LHC Computing Grid for delivering so effectively the computing infrastructure essential to our analyses. Finally, we acknowledge the enduring support for the construction and operation of the LHC and the CMS detector provided by the following funding agencies: BMWFW and FWF (Austria); FNRS and FWO (Belgium); CNPq, CAPES, FAPERJ, and FAPESP (Brazil); MES (Bulgaria); CERN; CAS, MoST, and NSFC (China); COLCIENCIAS (Colombia); MSES and CSF (Croatia); RPF (Cyprus); MoER, ERC IUT and ERDF (Estonia); Academy of Finland, MEC, and HIP (Finland); CEA and CNRS/IN2P3 (France); BMBF, DFG, and HGF (Germany); GSRT (Greece); OTKA and NIH (Hungary); DAE and DST (India); IPM (Iran); SFI (Ireland); INFN (Italy); MSIP and NRF (Republic of Korea); LAS (Lithuania); MOE and UM (Malaysia); CINVESTAV, CONACYT, SEP, and UASLP-FAI (Mexico); MBIE (New Zealand); PAEC (Pakistan); MSHE and NSC (Poland); FCT (Portugal); JINR (Dubna); MON, RosAtom, RAS and RFBR (Russia); MESTD (Serbia); SEIDI and CPAN (Spain); Swiss Funding Agencies (Switzerland); MST (Taipei); ThEPCenter, IPST, STAR and NSTDA (Thailand); TUBITAK and TAEK (Turkey); NASU and SFFR (Ukraine); STFC (United Kingdom); DOE and NSF (USA). Individuals have received support from the Marie-Curie program and the European Research Council and EPLANET (European Union); the Leventis Foundation; the A. P. Sloan Foundation; the Alexander von Humboldt Foundation; the Belgian Federal Science Policy Office; the Fonds pour la Formation à la Recherche dans l'Industrie et dans l'Agriculture (FRIA-Belgium); the Agentschap voor Innovatie door Wetenschap en Technologie (IWT-Belgium); the Ministry of Education, Youth and Sports (MEYS) of the Czech Republic; the Council of Science and Industrial Research, India; the HOMING PLUS program of the Foundation for Polish Science, cofinanced from European Union, Regional Development Fund; the OPUS program of the National Science Center (Poland); the Compagnia di San Paolo (Torino); MIUR project 20108T4XTM (Italy); the Thalís and Aristeia programs cofinanced by EU-ESF and the Greek NSRF; the National Priorities Research Program by Qatar National Research Fund; the Rachadapisek Sompot Fund for Postdoctoral Fellowship, Chulalongkorn University (Thailand); the Chulalongkorn Academic into Its 2nd Century Project Advancement Project (Thailand); and the Welch Foundation, contract C-1845.

References

- [1] P. Ramond, "Dual theory for free fermions", *Phys. Rev. D* **3** (1971) 2415, doi:10.1103/PhysRevD.3.2415.
- [2] Y. A. Golfand and E. P. Likhtman, "Extension of the algebra of Poincaré group generators and violation of P invariance", *JETP Lett.* **13** (1971) 323.
- [3] A. Neveu and J. H. Schwarz, "Factorizable dual model of pions", *Nucl. Phys. B* **31** (1971) 86, doi:10.1016/0550-3213(71)90448-2.
- [4] D. V. Volkov and V. P. Akulov, "Possible universal neutrino interaction", *JETP Lett.* **16** (1972) 438.
- [5] J. Wess and B. Zumino, "A Lagrangian model invariant under supergauge transformations", *Phys. Lett. B* **49** (1974) 52, doi:10.1016/0370-2693(74)90578-4.

- [6] J. Wess and B. Zumino, "Supergauge transformations in four dimensions", *Nucl. Phys. B* **70** (1974) 39, doi:10.1016/0550-3213(74)90355-1.
- [7] P. Fayet, "Supergauge invariant extension of the Higgs mechanism and a model for the electron and its neutrino", *Nucl. Phys. B* **90** (1975) 104, doi:10.1016/0550-3213(75)90636-7.
- [8] H. P. Nilles, "Supersymmetry, supergravity and particle physics", *Phys. Rep.* **110** (1984) 1, doi:10.1016/0370-1573(84)90008-5.
- [9] CMS Collaboration, "Search for supersymmetry in hadronic final states with missing transverse energy using the variables α_T and b-quark multiplicity in pp collisions at $\sqrt{s} = 8$ TeV", *Eur. Phys. J. C* **73** (2013) 2568, doi:10.1140/epjc/s10052-013-2568-6, arXiv:1303.2985.
- [10] CMS Collaboration, "Search for gluino mediated bottom- and top-squark production in multijet final states in pp collisions at 8 TeV", *Phys. Lett. B* **725** (2013) 243, doi:10.1016/j.physletb.2013.06.058, arXiv:1305.2390.
- [11] CMS Collaboration, "Search for new physics in the multijet and missing transverse momentum final state in proton-proton collisions at $\sqrt{s} = 8$ TeV", *JHEP* **06** (2014) 055, doi:10.1007/JHEP06(2014)055, arXiv:1402.4770.
- [12] CMS Collaboration, "Search for Supersymmetry using razor variables in events with b-tagged jets in pp collisions at $\sqrt{s} = 8$ TeV", *Phys. Rev. D* **91** (2015) 052018, doi:10.1103/PhysRevD.91.052018, arXiv:1502.00300.
- [13] CMS Collaboration, "Searches for supersymmetry using the M_{T2} variable in hadronic events produced in pp collisions at 8 TeV", *JHEP* **05** (2015) 078, doi:10.1007/JHEP05(2015)078, arXiv:1502.04358.
- [14] ATLAS Collaboration, "ATLAS Run 1 searches for direct pair production of third-generation squarks at the Large Hadron Collider", *Eur. Phys. J. C* **75** (2015) 510, doi:10.1140/epjc/s10052-015-3726-9, arXiv:1506.08616.
- [15] ATLAS Collaboration, "Summary of the searches for squarks and gluinos using $\sqrt{s} = 8$ TeV pp collisions with the ATLAS experiment at the LHC", *JHEP* **10** (2015) 054, doi:10.1007/JHEP10(2015)054, arXiv:1507.05525.
- [16] ATLAS Collaboration, "Search for new phenomena in final states with large jet multiplicities and missing transverse momentum with ATLAS using $\sqrt{s} = 13$ TeV proton-proton collisions", (2016). arXiv:1602.06194. Submitted to *Phys. Lett. B*.
- [17] CMS Collaboration, "Search for supersymmetry in the multijet and missing transverse momentum final state in pp collisions at 13 TeV", (2016). arXiv:1602.06581. Submitted to *Phys. Lett. B*.
- [18] C. G. Lester and D. J. Summers, "Measuring masses of semiinvisibly decaying particles pair produced at hadron colliders", *Phys. Lett. B* **463** (1999) 99, doi:10.1016/S0370-2693(99)00945-4, arXiv:hep-ph/9906349.
- [19] A. Barr, C. Lester, and P. Stephens, "m(T2): The truth behind the glamour", *J. Phys. G* **29** (2003) 2343, doi:10.1088/0954-3899/29/10/304, arXiv:hep-ph/0304226.

- [20] CMS Collaboration, “Search for supersymmetry in hadronic final states using M_{T2} in pp collisions at $\sqrt{s} = 7$ TeV”, *JHEP* **10** (2012) 018, doi:10.1007/JHEP10(2012)018, arXiv:1207.1798.
- [21] N. Arkani-Hamed et al., “MARMOSSET: The path from LHC data to the new standard model via on-shell effective theories”, (2007). arXiv:hep-ph/0703088.
- [22] J. Alwall, P. Schuster, and N. Toro, “Simplified models for a first characterization of new physics at the LHC”, *Phys. Rev. D* **79** (2009) 075020, doi:10.1103/PhysRevD.79.075020, arXiv:0810.3921.
- [23] J. Alwall, M.-P. Le, M. Lisanti, and J. G. Wacker, “Model-independent jets plus missing energy searches”, *Phys. Rev. D* **79** (2009) 015005, doi:10.1103/PhysRevD.79.015005, arXiv:0809.3264.
- [24] D. Alves et al., “Simplified models for LHC new physics searches”, *J. Phys. G* **39** (2012) 105005, doi:10.1088/0954-3899/39/10/105005, arXiv:1105.2838.
- [25] CMS Collaboration, “Interpretation of searches for supersymmetry with simplified models”, *Phys. Rev. D* **88** (2013) 052017, doi:10.1103/PhysRevD.88.052017, arXiv:1301.2175.
- [26] CMS Collaboration, “The CMS experiment at the CERN LHC”, *JINST* **3** (2008) S08004, doi:10.1088/1748-0221/3/08/S08004.
- [27] J. Alwall et al., “MadGraph 5: going beyond”, *JHEP* **06** (2011) 128, doi:10.1007/JHEP06(2011)128, arXiv:1106.0522.
- [28] T. Sjöstrand, S. Mrenna, and P. Z. Skands, “A brief introduction to PYTHIA 8.1”, *Comput. Phys. Commun.* **178** (2008) 852, doi:10.1016/j.cpc.2008.01.036, arXiv:0710.3820.
- [29] J. Alwall et al., “The automated computation of tree-level and next-to-leading order differential cross sections, and their matching to parton shower simulations”, *JHEP* **07** (2014) 079, doi:10.1007/JHEP07(2014)079, arXiv:1405.0301.
- [30] S. Alioli, P. Nason, C. Oleari, and E. Re, “NLO single-top production matched with shower in POWHEG: s - and t -channel contributions”, *JHEP* **09** (2009) 111, doi:10.1088/1126-6708/2009/09/111, arXiv:0907.4076. [Erratum: doi:10.1007/JHEP02(2010)011].
- [31] E. Re, “Single-top Wt -channel production matched with parton showers using the POWHEG method”, *Eur. Phys. J. C* **71** (2011) 1547, doi:10.1140/epjc/s10052-011-1547-z, arXiv:1009.2450.
- [32] R. Gavin, Y. Li, F. Petriello, and S. Quackenbush, “FEWZ 2.0: A code for hadronic Z production at next-to-next-to-leading order”, *Comput. Phys. Commun.* **182** (2011) 2388, doi:10.1016/j.cpc.2011.06.008, arXiv:1011.3540.
- [33] R. Gavin, Y. Li, F. Petriello, and S. Quackenbush, “W Physics at the LHC with FEWZ 2.1”, *Comput. Phys. Commun.* **184** (2013) 208, doi:10.1016/j.cpc.2012.09.005, arXiv:1201.5896.

- [34] M. Czakon and A. Mitov, "Top++: A program for the calculation of the top-pair cross-section at hadron colliders", *Comput. Phys. Commun.* **185** (2014) 2930, doi:10.1016/j.cpc.2014.06.021, arXiv:1112.5675.
- [35] C. Borschensky et al., "Squark and gluino production cross sections in pp collisions at $\sqrt{s} = 13, 14, 33$ and 100 TeV", *Eur. Phys. J. C* **74** (2014) 3174, doi:10.1140/epjc/s10052-014-3174-y, arXiv:1407.5066.
- [36] NNPDF Collaboration, "Parton distributions for the LHC Run II", *JHEP* **04** (2015) 040, doi:10.1007/JHEP04(2015)040, arXiv:1410.8849.
- [37] GEANT4 Collaboration, "GEANT4—a simulation toolkit", *Nucl. Instrum. Meth. A* **506** (2003) 250, doi:10.1016/S0168-9002(03)01368-8.
- [38] S. Abdullin et al., "The fast simulation of the CMS detector at LHC", *J. Phys. Conf. Ser.* **331** (2011) 032049, doi:10.1088/1742-6596/331/3/032049.
- [39] CMS Collaboration, "Particle-flow event reconstruction in CMS and performance for jets, taus, and E_T^{miss} ", CMS Physics Analysis Summary CMS-PAS-PFT-09-001, 2009.
- [40] CMS Collaboration, "Commissioning of the particle-flow event reconstruction with the first LHC collisions recorded in the CMS detector", CMS Physics Analysis Summary CMS-PAS-PFT-10-001, 2010.
- [41] M. Cacciari, G. P. Salam, and G. Soyez, "The anti- k_t jet clustering algorithm", *JHEP* **04** (2008) 063, doi:10.1088/1126-6708/2008/04/063, arXiv:0802.1189.
- [42] CMS Collaboration, "Determination of jet energy calibration and transverse momentum resolution in CMS", *JINST* **6** (2011) P11002, doi:10.1088/1748-0221/6/11/P11002, arXiv:1107.4277.
- [43] CMS Collaboration, "Performance of b-tagging algorithms in 25 ns data at 13 TeV", CMS Detector Performance Summary CMS-DP-2015-056, 2015.
- [44] CMS Collaboration, "Jet performance in pp collisions at $\sqrt{s} = 7$ TeV", CMS Physics Analysis Summary CMS-PAS-JME-10-003, 2010.
- [45] CMS Collaboration, "Performance of electron reconstruction and selection with the CMS detector in proton-proton collisions at $\sqrt{s} = 8$ TeV", *JINST* **10** (2015) P06005, doi:10.1088/1748-0221/10/06/P06005, arXiv:1502.02701.
- [46] CMS Collaboration, "Performance of CMS muon reconstruction in pp collision events at $\sqrt{s} = 7$ TeV", *JINST* **7** (2012) P10002, doi:10.1088/1748-0221/7/10/P10002, arXiv:1206.4071.
- [47] CMS Collaboration, "Study of pileup removal algorithms for jets", CMS Physics Analysis Summary CMS-PAS-JME-14-001, 2014.
- [48] CMS Collaboration, "Performance of photon reconstruction and identification with the CMS detector in proton-proton collisions at $\sqrt{s} = 8$ TeV", *JINST* **10** (2015) P08010, doi:10.1088/1748-0221/10/08/P08010, arXiv:1502.02702.
- [49] T. Sjöstrand, "The Lund Monte Carlo for e^+e^- jet physics", *Comput. Phys. Commun.* **28** (1983) 229, doi:10.1016/0010-4655(83)90041-3.

- [50] T. Sjöstrand, S. Mrenna, and P. Skands, “PYTHIA 6.4 physics and manual”, *JHEP* **05** (2006) 026, doi:10.1088/1126-6708/2006/05/026, arXiv:hep-ph/0603175.
- [51] UA1 Collaboration, “Experimental observation of isolated large transverse energy electrons with associated missing energy at $\sqrt{s} = 540$ GeV”, *Phys. Lett. B* **122** (1983) 103, doi:10.1016/0370-2693(83)91177-2.
- [52] CMS Collaboration, “Missing transverse energy performance of the CMS detector”, *JINST* **6** (2011) P09001, doi:10.1088/1748-0221/6/09/P09001, arXiv:1106.5048.
- [53] J. Butterworth et al., “PDF4LHC recommendations for LHC Run II”, *J. Phys. G* **43** (2016) 023001, doi:10.1088/0954-3899/43/2/023001, arXiv:1510.03865.
- [54] CMS Collaboration, “Search for new physics with same-sign isolated dilepton events with jets and missing transverse energy at the LHC”, *JHEP* **06** (2011) 077, doi:10.1007/JHEP06(2011)077, arXiv:1104.3168.
- [55] CMS Collaboration, “Search for new physics with jets and missing transverse momentum in pp collisions at $\sqrt{s} = 7$ TeV”, *JHEP* **08** (2011) 155, doi:10.1007/JHEP08(2011)155, arXiv:1106.4503.
- [56] Particle Data Group Collaboration, “Review of Particle Physics”, *Chin. Phys. C* **38** (2014) 090001, doi:10.1088/1674-1137/38/9/090001.
- [57] A. L. Read, “Presentation of search results: The CL_s technique”, *J. Phys. G* **28** (2002) 2693, doi:10.1088/0954-3899/28/10/313.
- [58] T. Junk, “Confidence level computation for combining searches with small statistics”, *Nucl. Instrum. Meth. A* **434** (1999) 435, doi:10.1016/S0168-9002(99)00498-2, arXiv:hep-ex/9902006.
- [59] G. Cowan, K. Cranmer, E. Gross, and O. Vitells, “Asymptotic formulae for likelihood-based tests of new physics”, *Eur. Phys. J. C* **71** (2011) 1554, doi:10.1140/epjc/s10052-011-1554-0, arXiv:1007.1727.
- [60] ATLAS and CMS Collaborations, “Procedure for the LHC Higgs boson search combination in summer 2011”, Technical Report ATL-PHYS-PUB-2011-011, CMS-NOTE-2011-005, 2011.
- [61] CMS Collaboration, “Search for top-squark pair production in the single-lepton final state in pp collisions at $\sqrt{s} = 8$ TeV”, *Eur. Phys. J. C* **73** (2013) 2677, doi:10.1140/epjc/s10052-013-2677-2, arXiv:1308.1586.
- [62] W. Beenakker, R. Höpker, M. Spira, and P. M. Zerwas, “Squark and gluino production at hadron colliders”, *Nucl. Phys. B* **492** (1997) 51, doi:10.1016/S0550-3213(97)00084-9, arXiv:hep-ph/9610490.
- [63] A. Kulesza and L. Motyka, “Threshold resummation for squark-antisquark and gluino-pair production at the LHC”, *Phys. Rev. Lett.* **102** (2009) 111802, doi:10.1103/PhysRevLett.102.111802, arXiv:0807.2405.
- [64] A. Kulesza and L. Motyka, “Soft gluon resummation for the production of gluino-gluino and squark-antisquark pairs at the LHC”, *Phys. Rev. D* **80** (2009) 095004, doi:10.1103/PhysRevD.80.095004, arXiv:0905.4749.

-
- [65] W. Beenakker et al., “Soft-gluon resummation for squark and gluino hadroproduction”, *JHEP* **12** (2009) 041, doi:10.1088/1126-6708/2009/12/041, arXiv:0909.4418.
- [66] W. Beenakker et al., “Squark and gluino hadroproduction”, *Int. J. Mod. Phys. A* **26** (2011) 2637, doi:10.1142/S0217751X11053560, arXiv:1105.1110.

A Detailed results

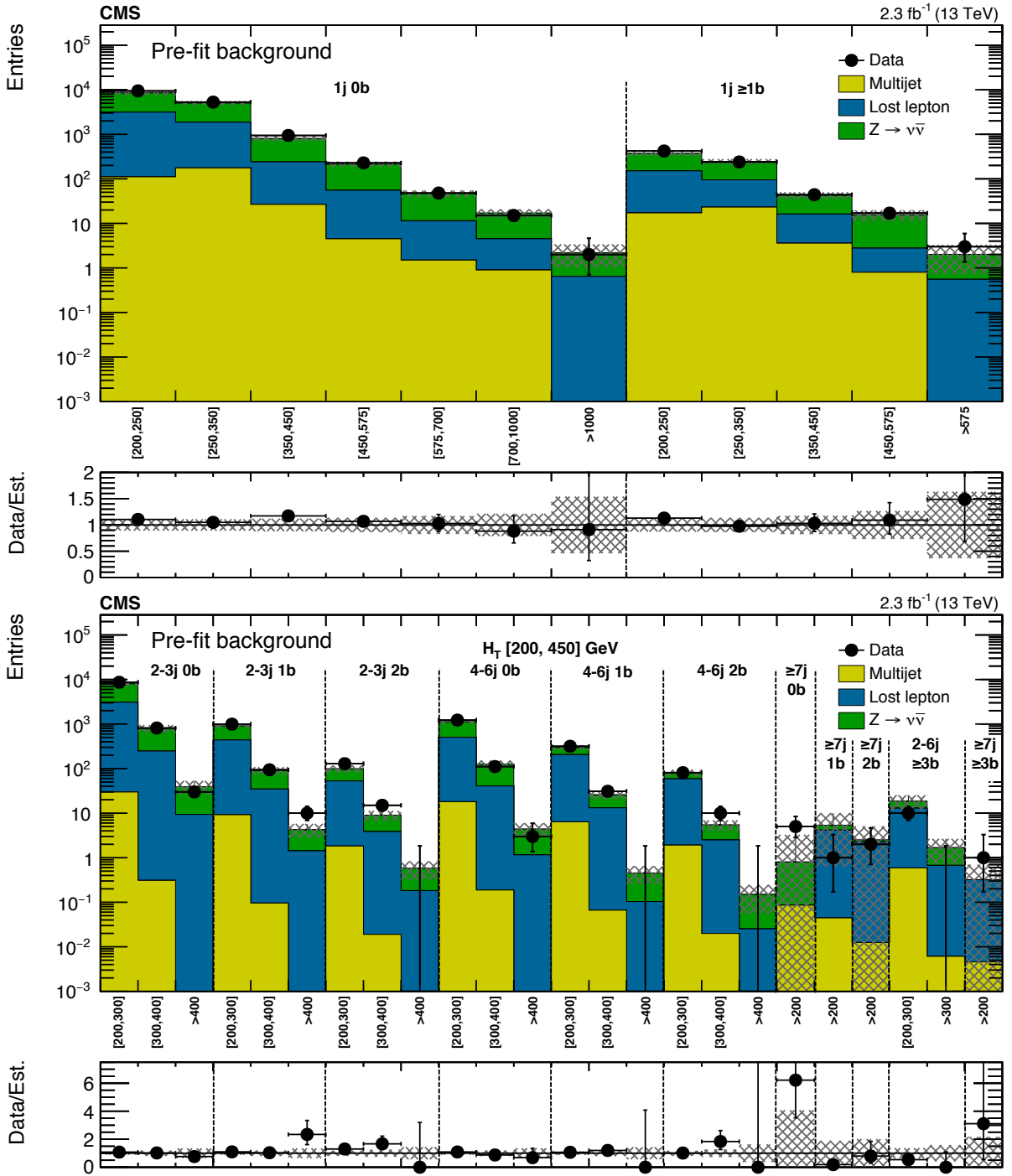


Figure A.1: (Above) Comparison of the estimated background (pre-fit) and observed data events in each signal bin in the monojet region. On the x -axis, the jet p_T binning is shown (in GeV). Hatched bands represent the full uncertainty in the background estimate. (Below) Same for the very-low- H_T region. On the x -axis, the M_{T2} binning is shown (in GeV). Bins with no entry for data have an observed count of 0 events.

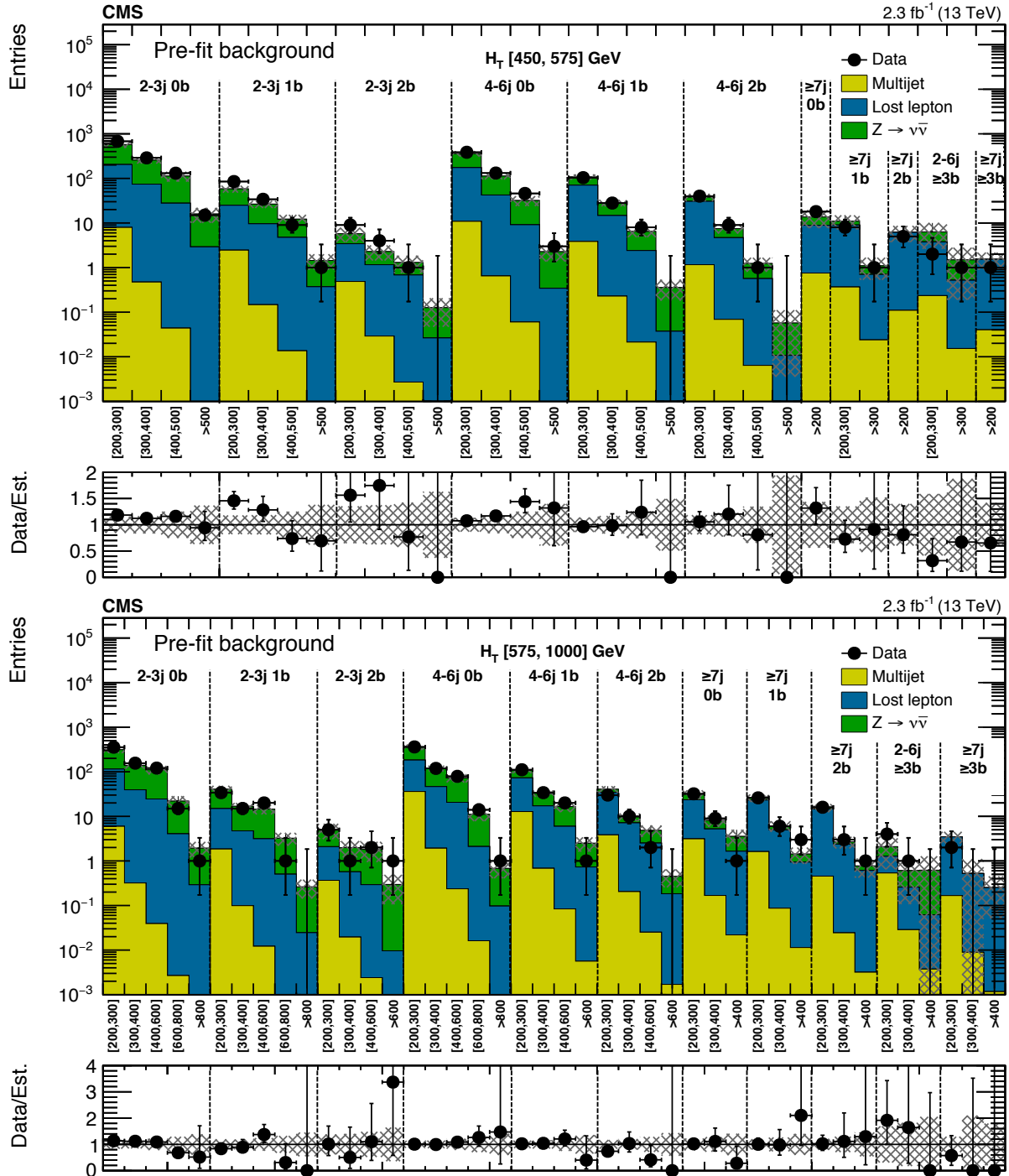


Figure A.2: (Above) Comparison of the estimated background (pre-fit) and observed data events in each signal bin in the low- H_T region. Hatched bands represent the full uncertainty in the background estimate. (Below) Same for the medium- H_T region. On the x -axis, the M_{T2} binning is shown (in GeV). Bins with no entry for data have an observed count of 0 events.

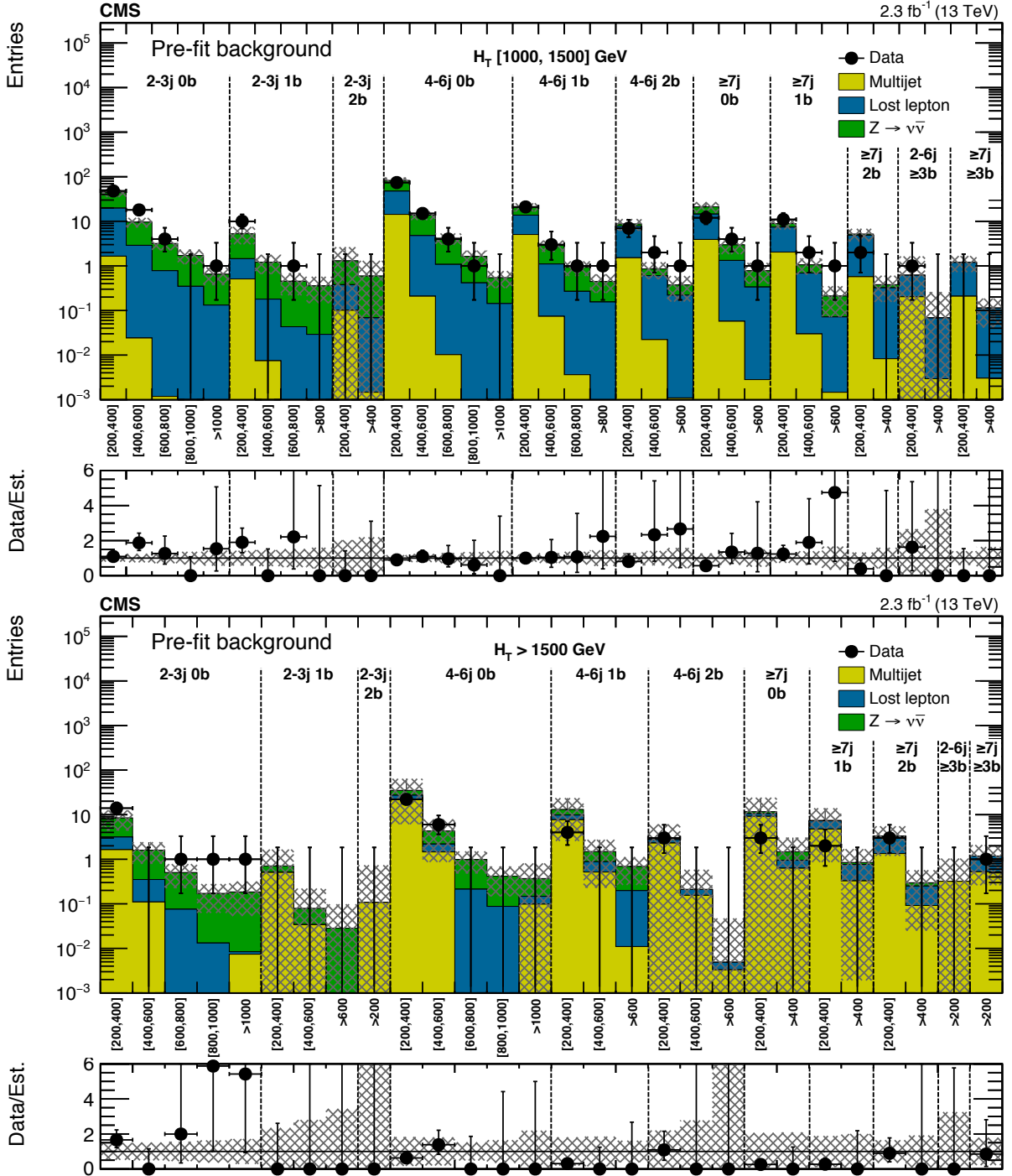


Figure A.3: (Above) Comparison of the estimated background (pre-fit) and observed data events in each signal bin in the high- H_T region. Hatched bands represent the full uncertainty in the background estimate. (Below) Same for the extreme- H_T region. On the x -axis, the M_{T2} binning is shown (in GeV). Bins with no entry for data have an observed count of 0 events.

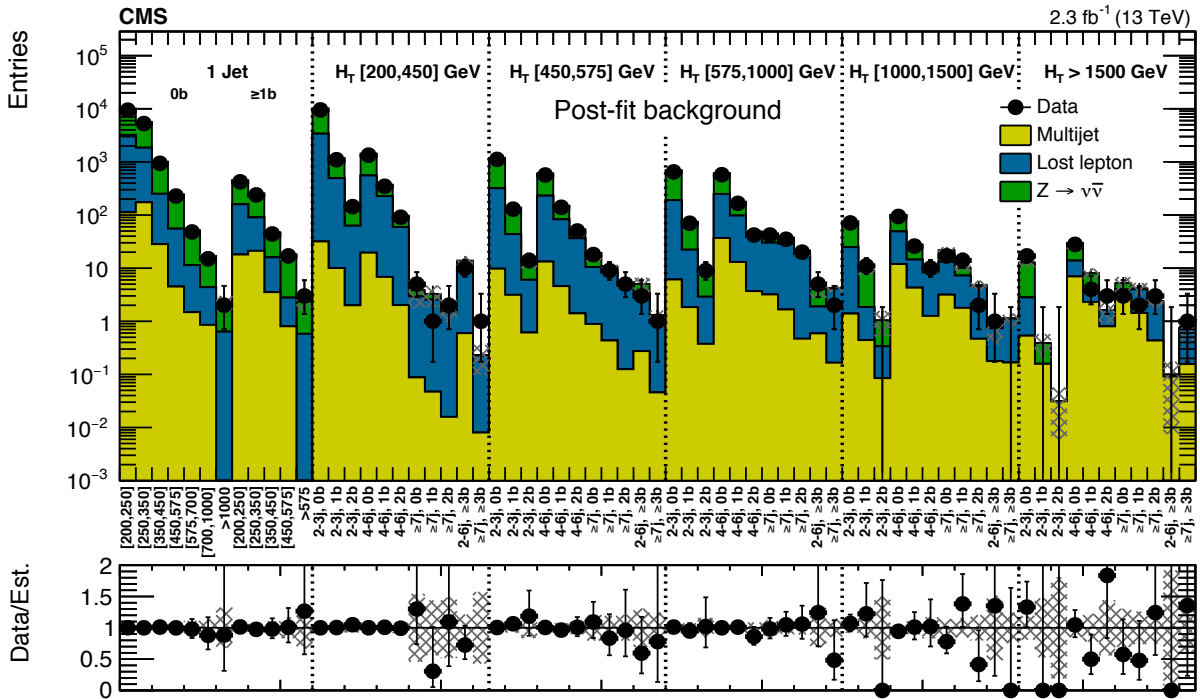


Figure A.4: Comparison of post-fit background prediction and observed data events in each topological region. Hatched bands represent the post-fit uncertainty in the background prediction. For the monojet region, on the x -axis, the jet p_T binning is shown in GeV.

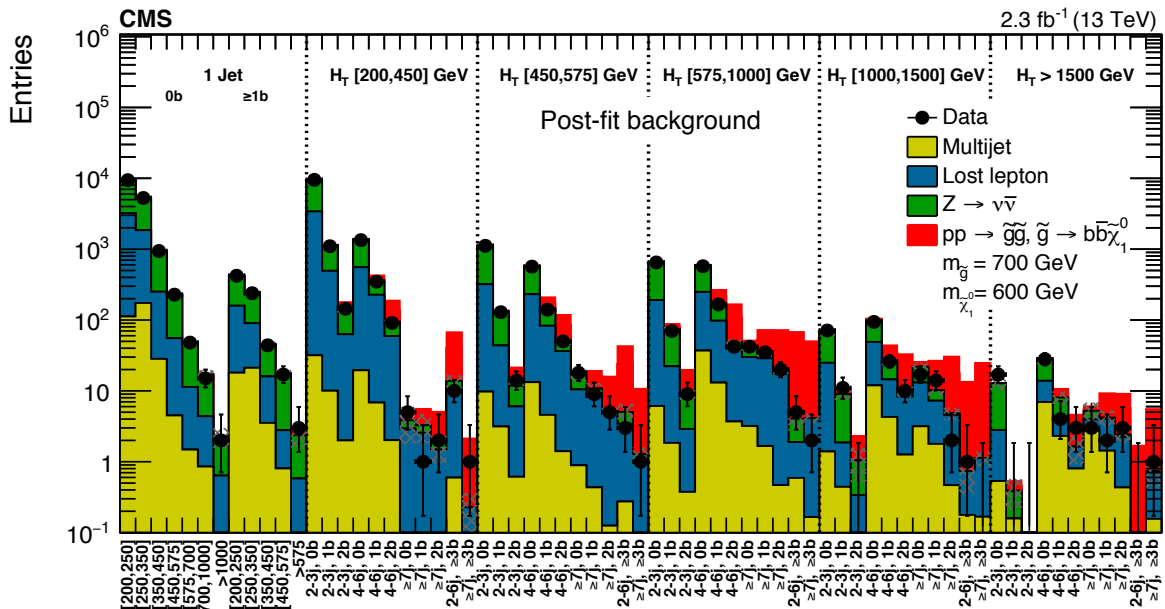


Figure A.5: Same as Fig. A.4 but also including the expected contribution from a compressed-spectrum signal model of gluino-mediated bottom squark production with the mass of the gluino and the LSP equal to 700 and 600 GeV, respectively. The signal model is described in Refs. [21–25] and in the text.

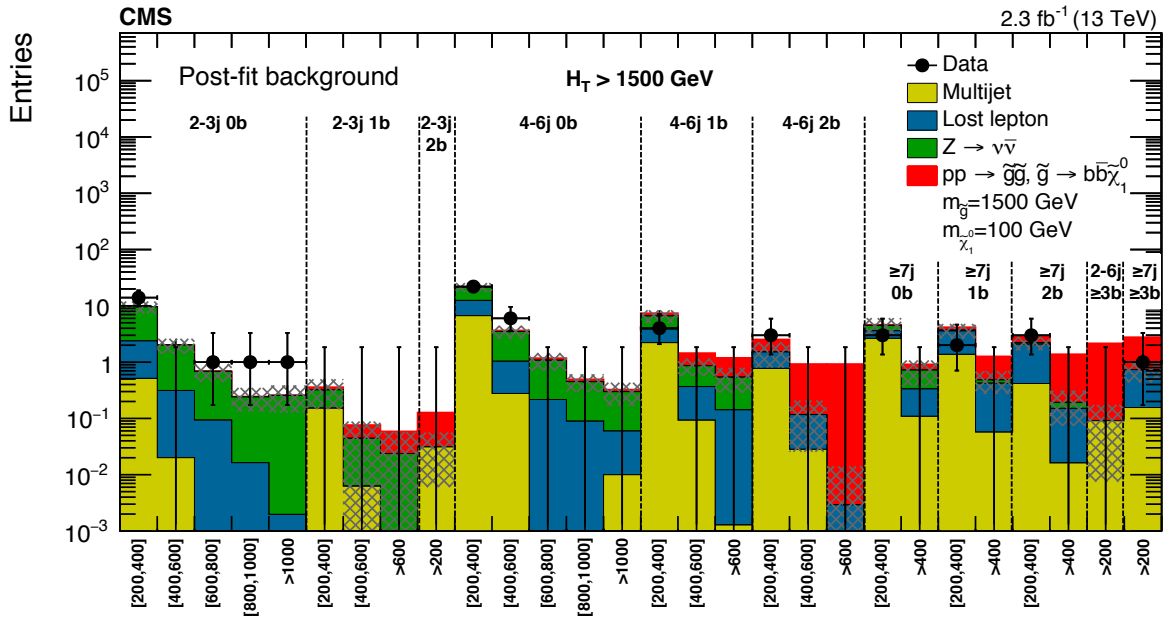


Figure A.6: Post-fit background prediction, expected signal yields, and observed data events in each signal bin in the extreme- H_T region. Hatched bands represent the post-fit uncertainty in the background prediction. On the x -axis, the M_{T2} binning is shown (in GeV). The red histogram shows the expected contribution from an open-spectra signal model of gluino-mediated bottom squark production with the mass of the gluino and the LSP equal to 1500 and 100 GeV, respectively. The signal model is described in Refs. [21–25] and in the text.

Table A.1: Binning in M_{T2} for each topological region of the multijet search regions with very low, low, and medium H_T .

H_T range [GeV]	Jet multiplicities	Bin boundaries [GeV]
200–450	2–3j, 0b	200–300, 300–400, >400
	2–3j, 1b	200–300, 300–400, >400
	2–3j, 2b	200–300, 300–400, >400
	4–6j, 0b	200–300, 300–400, >400
	4–6j, 1b	200–300, 300–400, >400
	4–6j, 2b	200–300, 300–400, >400
	$\geq 7j$, 0b	>200
	$\geq 7j$, 1b	>200
	$\geq 7j$, 2b	>200
	2–6j, $\geq 3b$	200–300, >300
	$\geq 7j$, $\geq 3b$	>200
450–575	2–3j, 0b	200–300, 300–400, 400–500, >500
	2–3j, 1b	200–300, 300–400, 400–500, >500
	2–3j, 2b	200–300, 300–400, 400–500, >500
	4–6j, 0b	200–300, 300–400, 400–500, >500
	4–6j, 1b	200–300, 300–400, 400–500, >500
	4–6j, 2b	200–300, 300–400, 400–500, >500
	$\geq 7j$, 0b	>200
	$\geq 7j$, 1b	200–300, >300
	$\geq 7j$, 2b	>200
	2–6j, $\geq 3b$	200–300, >300
	$\geq 7j$, $\geq 3b$	>200
575–1000	2–3j, 0b	200–300, 300–400, 400–600, 600–800, >800
	2–3j, 1b	200–300, 300–400, 400–600, 600–800, >800
	2–3j, 2b	200–300, 300–400, 400–600, >600
	4–6j, 0b	200–300, 300–400, 400–600, 600–800, >800
	4–6j, 1b	200–300, 300–400, 400–600, >600
	4–6j, 2b	200–300, 300–400, 400–600, >600
	$\geq 7j$, 0b	200–300, 300–400, >400
	$\geq 7j$, 1b	200–300, 300–400, >400
	$\geq 7j$, 2b	200–300, 300–400, >400
	2–6j, $\geq 3b$	200–300, 300–400, >400
	$\geq 7j$, $\geq 3b$	200–300, 300–400, >400

Table A.2: Binning in M_{T2} for each topological region of the multijet search regions with high and extreme H_T .

H_T range [GeV]	Jet multiplicities	Bin boundaries [GeV]	
1000–1500	2–3j, 0b	200–400, 400–600, 600–800, 800–1000, >1000	
	2–3j, 1b	200–400, 400–600, 600–800, >800	
	2–3j, 2b	200–400, >400	
	4–6j, 0b	200–400, 400–600, 600–800, 800–1000, >1000	
	4–6j, 1b	200–400, 400–600, 600–800, >800	
	4–6j, 2b	200–400, 400–600, >600	
	$\geq 7j$, 0b	200–400, 400–600, >600	
	$\geq 7j$, 1b	200–400, 400–600, >600	
	$\geq 7j$, 2b	200–400, >400	
	2–6j, $\geq 3b$	200–400, >400	
	$\geq 7j$, $\geq 3b$	200–400, >400	
	>1500	2–3j, 0b	200–400, 400–600, 600–800, 800–1000, >1000
		2–3j, 1b	200–400, 400–600, >600
2–3j, 2b		>200	
4–6j, 0b		200–400, 400–600, 600–800, 800–1000, >1000	
4–6j, 1b		200–400, 400–600, >600	
4–6j, 2b		200–400, 400–600, >600	
$\geq 7j$, 0b		200–400, >400	
$\geq 7j$, 1b		200–400, >400	
$\geq 7j$, 2b		200–400, >400	
2–6j, $\geq 3b$		>200	
$\geq 7j$, $\geq 3b$		>200	

Table A.3: Binning in jet p_T for the monojet regions.

Jet multiplicities	Bin boundaries [GeV]
1j, 0b	200–250, 250–350, 350–450, 450–575, 575–700, 700–1000, >1000
1j, $\geq 1b$	200–250, 250–350, 350–450, 450–575, >575

B Aggregated regions

To allow simpler reinterpretations, we also provide our results in “aggregated regions,” made from summing up the event yields and the pre-fit background predictions for individual signal bins in topologically similar regions. The uncertainty in the prediction in each aggregated region is calculated taking into account the same correlation model used in the full analysis. The definitions of these regions are given in Table B.1, while Table B.2 gives the predicted and observed number of events in each region together with the 95% CL upper limit on the number of signal events.

If these aggregated regions are used to derive cross section limits on the signals considered in this paper, they typically yield results that are less stringent by a factor of about two compared to the full binned analysis. This is shown in more detail for few signal models in Table B.3. The expected upper limit on the signal cross section as obtained from the full analysis is compared to the one obtained from the aggregated region that has the best sensitivity to the signal model considered. A 15% uncertainty in the signal selection efficiency is assumed for calculating these limits. The same table also provides the expected signal yields in the given aggregated regions.

Table B.1: Definitions of aggregated regions. Each aggregated region is obtained by selecting all events that pass the logical OR of the listed selections.

Region	N_j	N_b	H_T [GeV]	M_{T2} [GeV]
1j loose	=1	—	>450	—
	2-3	≤ 2	450-575	>400
	2-3	≤ 2	575-1000	>300
	2-3	≤ 2	>1000	>200
1j medium	=1	—	>575	—
	2-3	≤ 2	575-1000	>600
	2-3	≤ 2	>1000	>200
1j tight	=1	=0	>1000	—
	=1	≥ 1	>575	—
	2-3	=0	575-1000	>800
	2-3	1-2	575-1000	>600
	2-3	0-1	1000-1500	>800
	2-3	=2	1000-1500	>400
	2-3	0-1	>1500	>400
2j tight	2-3	—	>1000	>600
	2-3	—	>1500	>400
	4-6	—	>1000	>800
	4-6	—	>1500	>600
4j medium	≥ 4	—	>575	>400
4j tight	≥ 4	—	>1000	>600
	≥ 7	—	>1500	>400
7j tight	≥ 7	—	>575	>400
7j very tight	≥ 7	0-1	>1000	>600
	≥ 7	≥ 2	>1000	>400
	≥ 7	—	>1500	>400
2b medium	≥ 2	≥ 2	>575	>200
2b tight	≥ 2	≥ 2	>575	>400
2b very tight	≥ 2	≥ 2	>1000	>400
3b medium	≥ 2	≥ 3	>200	>200
3b tight	≥ 2	≥ 3	>575	>200
3b very tight	≥ 2	≥ 3	>1000	>200

Table B.2: Predictions and observations for the aggregated regions defined in Table B.1, together with the observed 95% CL limit on the number of signal events contributing to each region (N_{95}^{obs}). An uncertainty of either 15 or 30% in the signal efficiency is assumed for calculating the limits.

Region	Prediction	Observation	N_{95}^{obs} , 15% unc.	N_{95}^{obs} , 30% unc.
1j loose	833 ± 95	902	246	273
1j medium	175 ± 22	185	60	66
1j tight	$15.9^{+3.2}_{-2.9}$	12	7.9	8.4
2j tight	$15.7^{+4.0}_{-3.9}$	12	8.9	9.5
4j medium	159 ± 25	165	60	66
4j tight	$16.2^{+5.0}_{-4.9}$	11	8.7	9.3
7j tight	$15.3^{+4.6}_{-4.5}$	14	11	12
7j very tight	$5.3^{+3.3}_{-3.2}$	3	5.7	6.1
2b medium	119 ± 14	98	21	23
2b tight	$13.5^{+3.3}_{-3.1}$	10	7.7	8.2
2b very tight	$4.5^{+2.3}_{-2.1}$	4	6.3	6.8
3b medium	$40.9^{+9.9}_{-8.8}$	24	11	11
3b tight	$11.0^{+3.2}_{-2.5}$	9	7.7	8.2
3b very tight	$3.5^{+1.9}_{-1.4}$	2	4.3	4.5

Table B.3: Expected upper limits on the cross section of several signal models, as determined from the full binned analysis, are compared to the upper limits obtained using only the aggregated region that has the best sensitivity to each considered signal model. A 15% uncertainty in the signal selection efficiency is assumed for calculating these limits. The signal yields expected for an integrated luminosity of 2.3 fb^{-1} are also shown.

Signal	Expected limit [fb] (full analysis)	Best aggregated region	Signal yield (best aggregated region)	Expected limit [fb] (best aggregated region)
$pp \rightarrow \tilde{g}\tilde{g}, \tilde{g} \rightarrow b\bar{b}\tilde{\chi}_1^0$ ($m_{\tilde{g}} = 1700 \text{ GeV}, m_{\tilde{\chi}_1^0} = 0 \text{ GeV}$)	4.80	2b very tight	3.19	9.83
$pp \rightarrow \tilde{g}\tilde{g}, \tilde{g} \rightarrow b\bar{b}\tilde{\chi}_1^0$ ($m_{\tilde{g}} = 1000 \text{ GeV}, m_{\tilde{\chi}_1^0} = 950 \text{ GeV}$)	393	2b tight	4.79	667
$pp \rightarrow \tilde{g}\tilde{g}, \tilde{g} \rightarrow q\bar{q}\tilde{\chi}_1^0$ ($m_{\tilde{g}} = 1600 \text{ GeV}, m_{\tilde{\chi}_1^0} = 0 \text{ GeV}$)	8.67	4j tight	5.31	17.2
$pp \rightarrow \tilde{g}\tilde{g}, \tilde{g} \rightarrow q\bar{q}\tilde{\chi}_1^0$ ($m_{\tilde{g}} = 1000 \text{ GeV}, m_{\tilde{\chi}_1^0} = 850 \text{ GeV}$)	357	7j tight	7.33	536
$pp \rightarrow \tilde{g}\tilde{g}, \tilde{g} \rightarrow t\bar{t}\tilde{\chi}_1^0$ ($m_{\tilde{g}} = 1500 \text{ GeV}, m_{\tilde{\chi}_1^0} = 0 \text{ GeV}$)	12.9	7j very tight	4.48	20.7
$pp \rightarrow \tilde{g}\tilde{g}, \tilde{g} \rightarrow t\bar{t}\tilde{\chi}_1^0$ ($m_{\tilde{g}} = 900 \text{ GeV}, m_{\tilde{\chi}_1^0} = 600 \text{ GeV}$)	555	3b tight	5.55	1100
$pp \rightarrow \tilde{t}\tilde{t}, \tilde{t} \rightarrow t\tilde{\chi}_1^0$ ($m_{\tilde{t}} = 750 \text{ GeV}, m_{\tilde{\chi}_1^0} = 0 \text{ GeV}$)	41.8	2b tight	5.79	73.7
$pp \rightarrow \tilde{t}\tilde{t}, \tilde{t} \rightarrow t\tilde{\chi}_1^0$ ($m_{\tilde{t}} = 600 \text{ GeV}, m_{\tilde{\chi}_1^0} = 250 \text{ GeV}$)	151	2b medium	17.5	321
$pp \rightarrow \tilde{t}\tilde{t}, \tilde{t} \rightarrow t\tilde{\chi}_1^0$ ($m_{\tilde{t}} = 250 \text{ GeV}, m_{\tilde{\chi}_1^0} = 150 \text{ GeV}$)	18600	2b medium	9.37	73900
$pp \rightarrow \tilde{b}\tilde{b}, \tilde{b} \rightarrow b\tilde{\chi}_1^0$ ($m_{\tilde{b}} = 800 \text{ GeV}, m_{\tilde{\chi}_1^0} = 0 \text{ GeV}$)	26.9	2b tight	5.83	48.1
$pp \rightarrow \tilde{b}\tilde{b}, \tilde{b} \rightarrow b\tilde{\chi}_1^0$ ($m_{\tilde{b}} = 500 \text{ GeV}, m_{\tilde{\chi}_1^0} = 350 \text{ GeV}$)	451	2b medium	21.3	777
$pp \rightarrow \tilde{q}\tilde{q}, \tilde{q} \rightarrow q\tilde{\chi}_1^0, \tilde{q}_L + \tilde{q}_R(\tilde{u}, \tilde{d}, \tilde{s}, \tilde{c})$ ($m_{\tilde{q}} = 1200 \text{ GeV}, m_{\tilde{\chi}_1^0} = 0 \text{ GeV}$)	14.0	2j tight	7.85	18.3
$pp \rightarrow \tilde{q}\tilde{q}, \tilde{q} \rightarrow q\tilde{\chi}_1^0, \tilde{q}_L + \tilde{q}_R(\tilde{u}, \tilde{d}, \tilde{s}, \tilde{c})$ ($m_{\tilde{q}} = 600 \text{ GeV}, m_{\tilde{\chi}_1^0} = 0 \text{ GeV}$)	148	4j medium	300	267
$pp \rightarrow \tilde{q}\tilde{q}, \tilde{q} \rightarrow q\tilde{\chi}_1^0, \tilde{q}_L + \tilde{q}_R(\tilde{u}, \tilde{d}, \tilde{s}, \tilde{c})$ ($m_{\tilde{q}} = 700 \text{ GeV}, m_{\tilde{\chi}_1^0} = 500 \text{ GeV}$)	493	4j medium	34.0	902

C Summary plots

The figures in this appendix summarize in fewer bins the results shown in Figs 8, A.1, and A.2. The observed data are compared to estimated backgrounds as a function of M_{T2} in more inclusive regions. The aggregated regions presented in these figures are different from those in Appendix B, being instead formed by summing pre-fit values for all signal regions contained in the inclusive H_T, N_j, N_b selection displayed in the upper left corner of each plot.

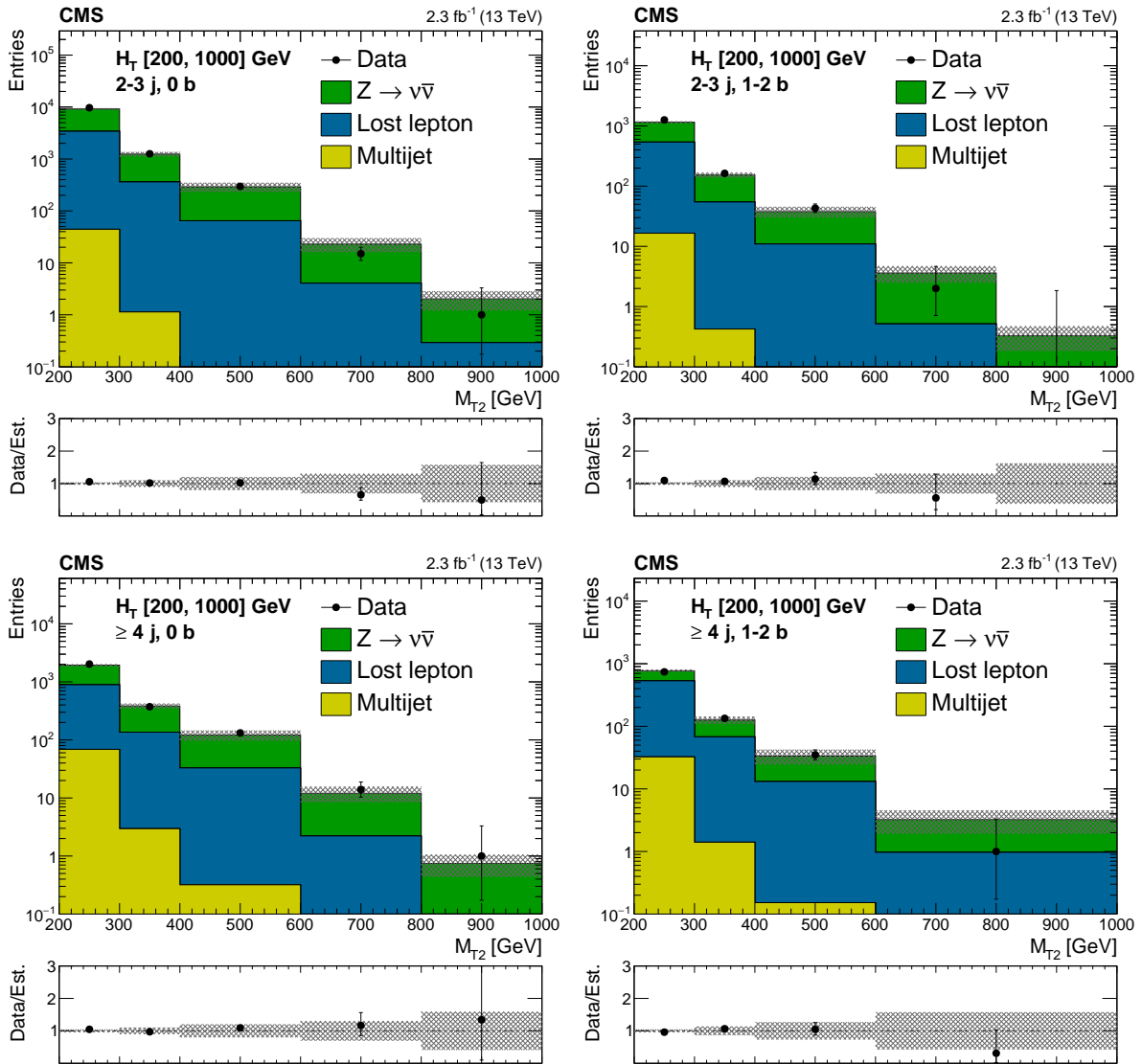


Figure C.1: Comparison of estimated background and observed data events in inclusive topological regions, as labeled in the legends, as a function of M_{T2} , for events with $200 < H_T < 1000$ GeV. The background prediction is formed by summing pre-fit values for all signal regions included in each plot. Hatched bands represent the full uncertainty in the background estimate.

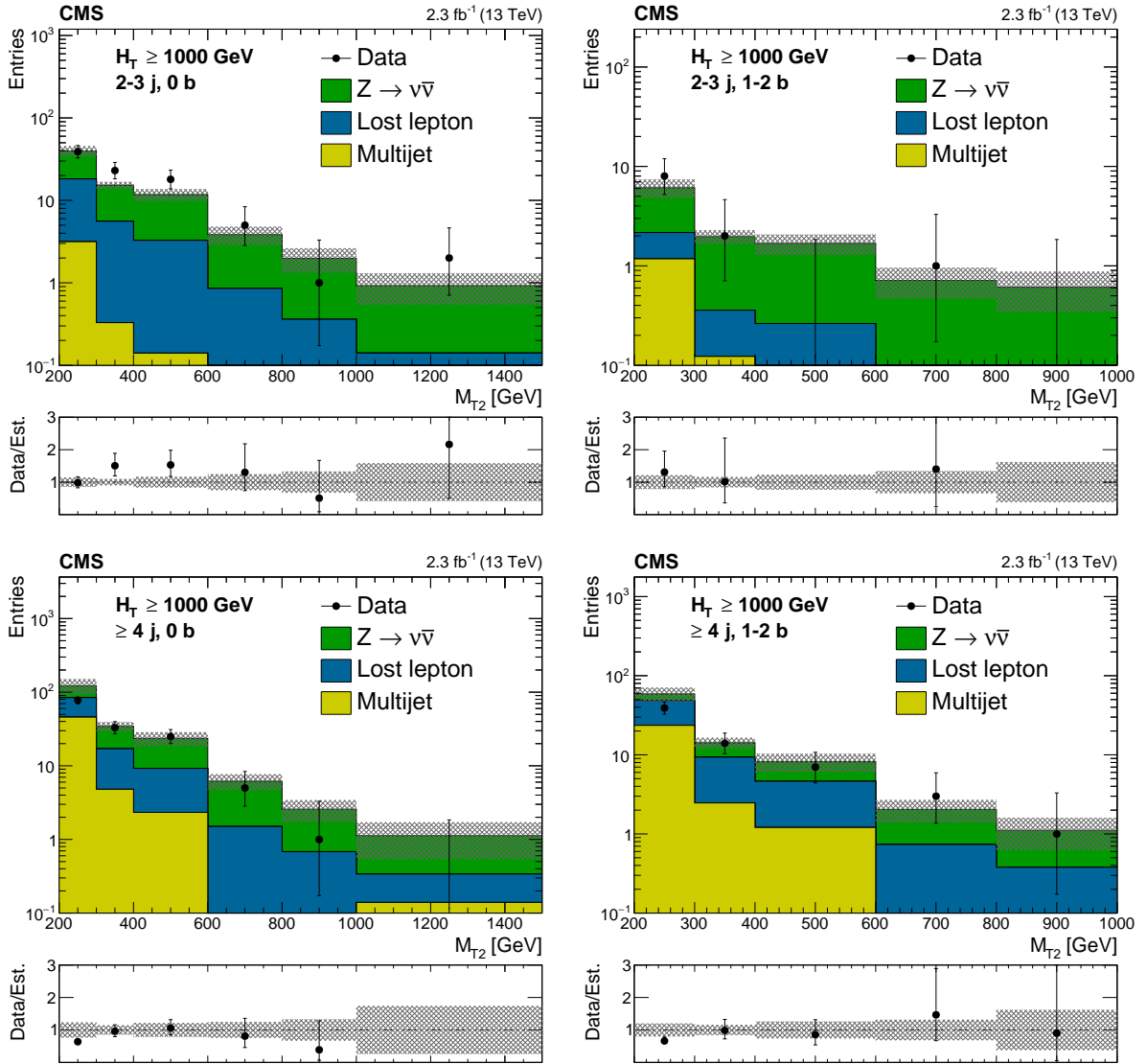


Figure C.2: Comparison of estimated background and observed data events in inclusive topological regions, as labeled in the legends, as a function of M_{T2} , for events with $H_T > 1000$ GeV. The background prediction is formed by summing pre-fit values for all signal regions included in each plot. Hatched bands represent the full uncertainty in the background estimate.

D The CMS Collaboration

Yerevan Physics Institute, Yerevan, Armenia

V. Khachatryan, A.M. Sirunyan, A. Tumasyan

Institut für Hochenergiephysik der OeAW, Wien, Austria

W. Adam, E. Asilar, T. Bergauer, J. Brandstetter, E. Brondolin, M. Dragicevic, J. Erö, M. Flechl, M. Friedl, R. Frühwirth¹, V.M. Ghete, C. Hartl, N. Hörmann, J. Hrubec, M. Jeitler¹, A. König, I. Krätschmer, D. Liko, T. Matsushita, I. Mikulec, D. Rabady, N. Rad, B. Rahbaran, H. Rohringer, J. Schieck¹, J. Strauss, W. Treberer-Treberspurg, W. Waltenberger, C.-E. Wulz¹

National Centre for Particle and High Energy Physics, Minsk, Belarus

V. Mossolov, N. Shumeiko, J. Suarez Gonzalez

Universiteit Antwerpen, Antwerpen, Belgium

S. Alderweireldt, T. Cornelis, E.A. De Wolf, X. Janssen, A. Knutsson, J. Lauwers, M. Van De Klundert, H. Van Haevermaet, P. Van Mechelen, N. Van Remortel, A. Van Spilbeeck

Vrije Universiteit Brussel, Brussel, Belgium

S. Abu Zeid, F. Blekman, J. D'Hondt, N. Daci, I. De Bruyn, K. Deroover, N. Heracleous, S. Lowette, S. Moortgat, L. Moreels, A. Olbrechts, Q. Python, S. Tavernier, W. Van Doninck, P. Van Mulders, I. Van Parijs

Université Libre de Bruxelles, Bruxelles, Belgium

H. Brun, C. Caillol, B. Clerbaux, G. De Lentdecker, H. Delannoy, G. Fasanella, L. Favart, R. Goldouzian, A. Grebenyuk, G. Karapostoli, T. Lenzi, A. Léonard, J. Luetic, T. Maerschalk, A. Marinov, A. Randle-conde, T. Seva, C. Vander Velde, P. Vanlaer, R. Yonamine, F. Zenoni, F. Zhang²

Ghent University, Ghent, Belgium

A. Cimmino, D. Dobur, A. Fagot, G. Garcia, M. Gul, J. Mccartin, D. Poyraz, S. Salva, R. Schöfbeck, M. Tytgat, W. Van Driessche, E. Yazgan, N. Zaganidis

Université Catholique de Louvain, Louvain-la-Neuve, Belgium

C. Beluffi³, O. Bondu, S. Brochet, G. Bruno, A. Caudron, L. Ceard, S. De Visscher, C. Delaere, M. Delcourt, L. Forthomme, B. Francois, A. Giammanco, A. Jafari, P. Jez, M. Komm, V. Lemaitre, A. Magitteri, A. Mertens, M. Musich, C. Nuttens, K. Piotrkowski, L. Quertenmont, M. Selvaggi, M. Vidal Marono, S. Wertz

Université de Mons, Mons, Belgium

N. Bely

Centro Brasileiro de Pesquisas Fisicas, Rio de Janeiro, Brazil

W.L. Aldá Júnior, F.L. Alves, G.A. Alves, L. Brito, M. Hamer, C. Hensel, A. Moraes, M.E. Pol, P. Rebello Teles

Universidade do Estado do Rio de Janeiro, Rio de Janeiro, Brazil

E. Belchior Batista Das Chagas, W. Carvalho, J. Chinellato⁴, A. Custódio, E.M. Da Costa, G.G. Da Silveira, D. De Jesus Damiao, C. De Oliveira Martins, S. Fonseca De Souza, L.M. Huertas Guativa, H. Malbouisson, D. Matos Figueiredo, C. Mora Herrera, L. Mundim, H. Nogima, W.L. Prado Da Silva, A. Santoro, A. Sznajder, E.J. Tonelli Manganote⁴, A. Vilela Pereira

Universidade Estadual Paulista ^a, Universidade Federal do ABC ^b, São Paulo, Brazil

S. Ahuja^a, C.A. Bernardes^b, S. Dogra^a, T.R. Fernandez Perez Tomei^a, E.M. Gregores^b,

P.G. Mercadante^b, C.S. Moon^{a,5}, S.F. Novaes^a, Sandra S. Padula^a, D. Romero Abad^b, J.C. Ruiz Vargas

Institute for Nuclear Research and Nuclear Energy, Sofia, Bulgaria

A. Aleksandrov, R. Hadjiiska, P. Iaydjiev, M. Rodozov, S. Stoykova, G. Sultanov, M. Vutova

University of Sofia, Sofia, Bulgaria

A. Dimitrov, I. Glushkov, L. Litov, B. Pavlov, P. Petkov

Beihang University, Beijing, China

W. Fang⁶

Institute of High Energy Physics, Beijing, China

M. Ahmad, J.G. Bian, G.M. Chen, H.S. Chen, M. Chen, Y. Chen⁷, T. Cheng, R. Du, C.H. Jiang, D. Leggat, Z. Liu, F. Romeo, S.M. Shaheen, A. Spiezia, J. Tao, C. Wang, Z. Wang, H. Zhang, J. Zhao

State Key Laboratory of Nuclear Physics and Technology, Peking University, Beijing, China

C. Asawatangtrakuldee, Y. Ban, Q. Li, S. Liu, Y. Mao, S.J. Qian, D. Wang, Z. Xu

Universidad de Los Andes, Bogota, Colombia

C. Avila, A. Cabrera, L.F. Chaparro Sierra, C. Florez, J.P. Gomez, C.F. González Hernández, J.D. Ruiz Alvarez, J.C. Sanabria

University of Split, Faculty of Electrical Engineering, Mechanical Engineering and Naval Architecture, Split, Croatia

N. Godinovic, D. Lelas, I. Puljak, P.M. Ribeiro Cipriano

University of Split, Faculty of Science, Split, Croatia

Z. Antunovic, M. Kovac

Institute Rudjer Boskovic, Zagreb, Croatia

V. Brigljevic, D. Ferencek, K. Kadija, S. Micanovic, L. Sudic

University of Cyprus, Nicosia, Cyprus

A. Attikis, G. Mavromanolakis, J. Mousa, C. Nicolaou, F. Ptochos, P.A. Razis, H. Rykaczewski

Charles University, Prague, Czech Republic

M. Finger⁸, M. Finger Jr.⁸

Universidad San Francisco de Quito, Quito, Ecuador

E. Carrera Jarrin

Academy of Scientific Research and Technology of the Arab Republic of Egypt, Egyptian Network of High Energy Physics, Cairo, Egypt

A.A. Abdelalim^{9,10}, E. El-khateeb^{11,11}, A.M. Kuotb Awad¹², E. Salama^{13,11}

National Institute of Chemical Physics and Biophysics, Tallinn, Estonia

B. Calpas, M. Kadastik, M. Murumaa, L. Perrini, M. Raidal, A. Tiko, C. Veelken

Department of Physics, University of Helsinki, Helsinki, Finland

P. Eerola, J. Pekkanen, M. Voutilainen

Helsinki Institute of Physics, Helsinki, Finland

J. Härkönen, V. Karimäki, R. Kinnunen, T. Lampén, K. Lassila-Perini, S. Lehti, T. Lindén, P. Luukka, T. Peltola, J. Tuominiemi, E. Tuovinen, L. Wendland

Lappeenranta University of Technology, Lappeenranta, Finland

J. Talvitie, T. Tuuva

DSM/IRFU, CEA/Saclay, Gif-sur-Yvette, France

M. Besancon, F. Couderc, M. Dejardin, D. Denegri, B. Fabbro, J.L. Faure, C. Favaro, F. Ferri, S. Ganjour, S. Ghosh, A. Givernaud, P. Gras, G. Hamel de Monchenault, P. Jarry, I. Kucher, E. Locci, M. Machet, J. Malcles, J. Rander, A. Rosowsky, M. Titov, A. Zghiche

Laboratoire Leprince-Ringuet, Ecole Polytechnique, IN2P3-CNRS, Palaiseau, France

A. Abdulsalam, I. Antropov, S. Baffioni, F. Beaudette, P. Busson, L. Cadamuro, E. Chapon, C. Charlot, O. Davignon, R. Granier de Cassagnac, M. Jo, S. Lisniak, P. Miné, I.N. Naranjo, M. Nguyen, C. Ochando, G. Ortona, P. Paganini, P. Pigard, S. Regnard, R. Salerno, Y. Sirois, T. Strebler, Y. Yilmaz, A. Zabi

Institut Pluridisciplinaire Hubert Curien, Université de Strasbourg, Université de Haute Alsace Mulhouse, CNRS/IN2P3, Strasbourg, France

J.-L. Agram¹⁴, J. Andrea, A. Aubin, D. Bloch, J.-M. Brom, M. Buttignol, E.C. Chabert, N. Chanon, C. Collard, E. Conte¹⁴, X. Coubez, J.-C. Fontaine¹⁴, D. Gelé, U. Goerlach, A.-C. Le Bihan, J.A. Merlin¹⁵, K. Skovpen, P. Van Hove

Centre de Calcul de l'Institut National de Physique Nucleaire et de Physique des Particules, CNRS/IN2P3, Villeurbanne, France

S. Gadrat

Université de Lyon, Université Claude Bernard Lyon 1, CNRS-IN2P3, Institut de Physique Nucléaire de Lyon, Villeurbanne, France

S. Beauceron, C. Bernet, G. Boudoul, E. Bouvier, C.A. Carrillo Montoya, R. Chierici, D. Contardo, B. Courbon, P. Depasse, H. El Mamouni, J. Fan, J. Fay, S. Gascon, M. Gouzevitch, G. Grenier, B. Ille, F. Lagarde, I.B. Laktineh, M. Lethuillier, L. Mirabito, A.L. Pequegnot, S. Perries, A. Popov¹⁶, D. Sabes, V. Sordini, M. Vander Donckt, P. Verdier, S. Viret

Georgian Technical University, Tbilisi, Georgia

A. Khvedelidze⁸

Tbilisi State University, Tbilisi, Georgia

Z. Tsamalaidze⁸

RWTH Aachen University, I. Physikalisches Institut, Aachen, Germany

C. Autermann, S. Beranek, L. Feld, A. Heister, M.K. Kiesel, K. Klein, M. Lipinski, A. Ostapchuk, M. Preuten, F. Raupach, S. Schael, C. Schomakers, J.F. Schulte, J. Schulz, T. Verlage, H. Weber, V. Zhukov¹⁶

RWTH Aachen University, III. Physikalisches Institut A, Aachen, Germany

M. Brodski, E. Dietz-Laursonn, D. Duchardt, M. Endres, M. Erdmann, S. Erdweg, T. Esch, R. Fischer, A. Güth, T. Hebbeker, C. Heidemann, K. Hoepfner, S. Knutzen, M. Merschmeyer, A. Meyer, P. Millet, S. Mukherjee, M. Olschewski, K. Padeken, P. Papacz, T. Pook, M. Radziej, H. Reithler, M. Rieger, F. Scheuch, L. Sonnenschein, D. Teysier, S. Thüer

RWTH Aachen University, III. Physikalisches Institut B, Aachen, Germany

V. Cherepanov, Y. Erdogan, G. Flügge, F. Hoehle, B. Kargoll, T. Kress, A. Künsken, J. Lingemann, A. Nehr Korn, A. Nowack, I.M. Nugent, C. Pistone, O. Pooth, A. Stahl¹⁵

Deutsches Elektronen-Synchrotron, Hamburg, Germany

M. Aldaya Martin, I. Asin, K. Beernaert, O. Behnke, U. Behrens, A.A. Bin Anuar, K. Borrás¹⁷, A. Campbell, P. Connor, C. Contreras-Campana, F. Costanza, C. Diez Pardos,

G. Dolinska, G. Eckerlin, D. Eckstein, T. Eichhorn, E. Gallo¹⁸, J. Garay Garcia, A. Geiser, A. Gizhko, J.M. Grados Luyando, P. Gunnellini, A. Harb, J. Hauk, M. Hempel¹⁹, H. Jung, A. Kalogeropoulos, O. Karacheban¹⁹, M. Kasemann, J. Keaveney, J. Kieseler, C. Kleinwort, I. Korol, W. Lange, A. Lelek, J. Leonard, K. Lipka, A. Lobanov, W. Lohmann¹⁹, R. Mankel, I.-A. Melzer-Pellmann, A.B. Meyer, G. Mittag, J. Mnich, A. Mussgiller, E. Ntomari, D. Pitzl, R. Placakyte, A. Raspereza, B. Roland, M.Ö. Sahin, P. Saxena, T. Schoerner-Sadenius, C. Seitz, S. Spannagel, N. Stefaniuk, K.D. Trippkewitz, G.P. Van Onsem, R. Walsh, C. Wissing

University of Hamburg, Hamburg, Germany

V. Blobel, M. Centis Vignali, A.R. Draeger, T. Dreyer, J. Erfle, E. Garutti, K. Goebel, D. Gonzalez, M. Görner, J. Haller, M. Hoffmann, R.S. Höing, A. Junkes, R. Klanner, R. Kogler, N. Kovalchuk, T. Lapsien, T. Lenz, I. Marchesini, D. Marconi, M. Meyer, M. Niedziela, D. Nowatschin, J. Ott, F. Pantaleo¹⁵, T. Peiffer, A. Perieanu, N. Pietsch, J. Poehlsen, C. Sander, C. Scharf, P. Schleper, E. Schlieckau, A. Schmidt, S. Schumann, J. Schwandt, H. Stadie, G. Steinbrück, F.M. Stober, M. Stöver, H. Tholen, D. Troendle, E. Usai, L. Vaneldereren, A. Vanhoefer, B. Vormwald

Institut für Experimentelle Kernphysik, Karlsruhe, Germany

C. Barth, C. Baus, J. Berger, E. Butz, T. Chwalek, F. Colombo, W. De Boer, A. Dierlamm, S. Fink, R. Friese, M. Giffels, A. Gilbert, D. Haitz, F. Hartmann¹⁵, S.M. Heindl, U. Husemann, I. Katkov¹⁶, A. Kornmayer¹⁵, P. Lobelle Pardo, B. Maier, H. Mildner, M.U. Mozer, T. Müller, Th. Müller, M. Plagge, G. Quast, K. Rabbertz, S. Röcker, F. Roscher, M. Schröder, G. Sieber, H.J. Simonis, R. Ulrich, J. Wagner-Kuhr, S. Wayand, M. Weber, T. Weiler, S. Williamson, C. Wöhrmann, R. Wolf

Institute of Nuclear and Particle Physics (INPP), NCSR Demokritos, Aghia Paraskevi, Greece

G. Anagnostou, G. Daskalakis, T. Gerasis, V.A. Giakoumopoulou, A. Kyriakis, D. Loukas, I. Topsis-Giotis

National and Kapodistrian University of Athens, Athens, Greece

A. Agapitos, S. Kesisoglou, A. Panagiotou, N. Saoulidou, E. Tziaferi

University of Ioánnina, Ioánnina, Greece

I. Evangelou, G. Flouris, C. Foudas, P. Kokkas, N. Loukas, N. Manthos, I. Papadopoulos, E. Paradis

MTA-ELTE Lendület CMS Particle and Nuclear Physics Group, Eötvös Loránd University

N. Filipovic

Wigner Research Centre for Physics, Budapest, Hungary

G. Bencze, C. Hajdu, P. Hidas, D. Horvath²⁰, F. Sikler, V. Veszpremi, G. Vesztergombi²¹, A.J. Zsigmond

Institute of Nuclear Research ATOMKI, Debrecen, Hungary

N. Beni, S. Czellar, J. Karancsi²², J. Molnar, Z. Szillasi

University of Debrecen, Debrecen, Hungary

M. Bartók²¹, A. Makovec, P. Raics, Z.L. Trocsanyi, B. Ujvari

National Institute of Science Education and Research, Bhubaneswar, India

S. Bahinipati, S. Choudhury²³, P. Mal, K. Mandal, A. Nayak²⁴, D.K. Sahoo, N. Sahoo, S.K. Swain

Panjab University, Chandigarh, India

S. Bansal, S.B. Beri, V. Bhatnagar, R. Chawla, R. Gupta, U. Bhawandeep, A.K. Kalsi, A. Kaur, M. Kaur, R. Kumar, A. Mehta, M. Mittal, J.B. Singh, G. Walia

University of Delhi, Delhi, India

Ashok Kumar, A. Bhardwaj, B.C. Choudhary, R.B. Garg, S. Keshri, A. Kumar, S. Malhotra, M. Naimuddin, N. Nishu, K. Ranjan, R. Sharma, V. Sharma

Saha Institute of Nuclear Physics, Kolkata, India

R. Bhattacharya, S. Bhattacharya, K. Chatterjee, S. Dey, S. Dutt, S. Dutta, S. Ghosh, N. Majumdar, A. Modak, K. Mondal, S. Mukhopadhyay, S. Nandan, A. Purohit, A. Roy, D. Roy, S. Roy Chowdhury, S. Sarkar, M. Sharan, S. Thakur

Indian Institute of Technology Madras, Madras, India

P.K. Behera

Bhabha Atomic Research Centre, Mumbai, India

R. Chudasama, D. Dutta, V. Jha, V. Kumar, A.K. Mohanty¹⁵, P.K. Netrakanti, L.M. Pant, P. Shukla, A. Topkar

Tata Institute of Fundamental Research-A, Mumbai, India

T. Aziz, S. Dugad, G. Kole, B. Mahakud, S. Mitra, G.B. Mohanty, P. Shingade, R. Shukla, N. Sur, B. Sutar

Tata Institute of Fundamental Research-B, Mumbai, India

S. Banerjee, S. Bhowmik²⁵, R.K. Dewanjee, S. Ganguly, M. Guchait, Sa. Jain, S. Kumar, M. Maity²⁵, G. Majumder, K. Mazumdar, B. Parida, T. Sarkar²⁵, N. Wickramage²⁶

Indian Institute of Science Education and Research (IISER), Pune, India

S. Chauhan, S. Dube, A. Kapoor, K. Kothekar, A. Rane, S. Sharma

Institute for Research in Fundamental Sciences (IPM), Tehran, Iran

H. Bakhshiansohi, H. Behnamian, S. Chenarani²⁷, E. Eskandari Tadavani, S.M. Etesami²⁷, A. Fahim²⁸, M. Khakzad, M. Mohammadi Najafabadi, M. Naseri, S. Paktinat Mehdiabadi, F. Rezaei Hosseinabadi, B. Safarzadeh²⁹, M. Zeinali

University College Dublin, Dublin, Ireland

M. Felcini, M. Grunewald

INFN Sezione di Bari ^a, Università di Bari ^b, Politecnico di Bari ^c, Bari, Italy

M. Abbrescia^{a,b}, C. Calabria^{a,b}, C. Caputo^{a,b}, A. Colaleo^a, D. Creanza^{a,c}, L. Cristella^{a,b}, N. De Filippis^{a,c}, M. De Palma^{a,b}, L. Fiore^a, G. Iaselli^{a,c}, G. Maggi^{a,c}, M. Maggi^a, G. Miniello^{a,b}, S. My^{a,b}, S. Nuzzo^{a,b}, A. Pompili^{a,b}, G. Pugliese^{a,c}, R. Radogna^{a,b}, A. Ranieri^a, G. Selvaggi^{a,b}, L. Silvestris^{a,15}, R. Venditti^{a,b}

INFN Sezione di Bologna ^a, Università di Bologna ^b, Bologna, Italy

G. Abbiendi^a, C. Battilana, D. Bonacorsi^{a,b}, S. Braibant-Giacomelli^{a,b}, L. Brigliadori^{a,b}, R. Campanini^{a,b}, P. Capiluppi^{a,b}, A. Castro^{a,b}, F.R. Cavallo^a, S.S. Chhibra^{a,b}, G. Codispoti^{a,b}, M. Cuffiani^{a,b}, G.M. Dallavalle^a, F. Fabbri^a, A. Fanfani^{a,b}, D. Fasanella^{a,b}, P. Giacomelli^a, C. Grandi^a, L. Guiducci^{a,b}, S. Marcellini^a, G. Masetti^a, A. Montanari^a, F.L. Navarra^{a,b}, A. Perrotta^a, A.M. Rossi^{a,b}, T. Rovelli^{a,b}, G.P. Siroli^{a,b}, N. Tosi^{a,b,15}

INFN Sezione di Catania ^a, Università di Catania ^b, Catania, Italy

S. Albergo^{a,b}, M. Chiorboli^{a,b}, S. Costa^{a,b}, A. Di Mattia^a, F. Giordano^{a,b}, R. Potenza^{a,b}, A. Tricomi^{a,b}, C. Tuve^{a,b}

INFN Sezione di Firenze ^a, Università di Firenze ^b, Firenze, Italy

G. Barbagli^a, V. Ciulli^{a,b}, C. Civinini^a, R. D'Alessandro^{a,b}, E. Focardi^{a,b}, V. Gori^{a,b}, P. Lenzi^{a,b}, M. Meschini^a, S. Paoletti^a, G. Sguazzoni^a, L. Viliani^{a,b,15}

INFN Laboratori Nazionali di Frascati, Frascati, Italy

L. Benussi, S. Bianco, F. Fabbri, D. Piccolo, F. Primavera¹⁵

INFN Sezione di Genova ^a, Università di Genova ^b, Genova, Italy

V. Calvelli^{a,b}, F. Ferro^a, M. Lo Vetere^{a,b}, M.R. Monge^{a,b}, E. Robutti^a, S. Tosi^{a,b}

INFN Sezione di Milano-Bicocca ^a, Università di Milano-Bicocca ^b, Milano, Italy

L. Brianza, M.E. Dinardo^{a,b}, S. Fiorendi^{a,b}, S. Gennai^a, A. Ghezzi^{a,b}, P. Govoni^{a,b}, S. Malvezzi^a, R.A. Manzoni^{a,b,15}, B. Marzocchi^{a,b}, D. Menasce^a, L. Moroni^a, M. Paganoni^{a,b}, D. Pedrini^a, S. Pigazzini, S. Ragazzi^{a,b}, T. Tabarelli de Fatis^{a,b}

INFN Sezione di Napoli ^a, Università di Napoli 'Federico II' ^b, Napoli, Italy, Università della Basilicata ^c, Potenza, Italy, Università G. Marconi ^d, Roma, Italy

S. Buontempo^a, N. Cavallo^{a,c}, G. De Nardo, S. Di Guida^{a,d,15}, M. Esposito^{a,b}, F. Fabozzi^{a,c}, A.O.M. Iorio^{a,b}, G. Lanza^a, L. Lista^a, S. Meola^{a,d,15}, M. Merola^a, P. Paolucci^{a,15}, C. Sciacca^{a,b}, F. Thyssen

INFN Sezione di Padova ^a, Università di Padova ^b, Padova, Italy, Università di Trento ^c, Trento, Italy

P. Azzi^{a,15}, N. Bacchetta^a, L. Benato^{a,b}, D. Bisello^{a,b}, A. Boletti^{a,b}, R. Carlin^{a,b}, A. Carvalho Antunes De Oliveira^{a,b}, P. Checchia^a, M. Dall'Osso^{a,b}, P. De Castro Manzano^a, T. Dorigo^a, U. Dosselli^a, F. Gasparini^{a,b}, U. Gasparini^{a,b}, A. Gozzelino^a, S. Lacaprara^a, M. Margoni^{a,b}, A.T. Meneguzzo^{a,b}, J. Pazzini^{a,b,15}, N. Pozzobon^{a,b}, P. Ronchese^{a,b}, F. Simonetto^{a,b}, E. Torassa^a, M. Tosi^{a,b}, M. Zanetti, P. Zotto^{a,b}, A. Zucchetta^{a,b}, G. Zumerle^{a,b}

INFN Sezione di Pavia ^a, Università di Pavia ^b, Pavia, Italy

A. Braghieri^a, A. Magnani^{a,b}, P. Montagna^{a,b}, S.P. Ratti^{a,b}, V. Re^a, C. Riccardi^{a,b}, P. Salvini^a, I. Vai^{a,b}, P. Vitulo^{a,b}

INFN Sezione di Perugia ^a, Università di Perugia ^b, Perugia, Italy

L. Alunni Solestizi^{a,b}, G.M. Bilei^a, D. Ciangottini^{a,b}, L. Fanò^{a,b}, P. Lariccia^{a,b}, R. Leonardi^{a,b}, G. Mantovani^{a,b}, M. Menichelli^a, A. Saha^a, A. Santocchia^{a,b}

INFN Sezione di Pisa ^a, Università di Pisa ^b, Scuola Normale Superiore di Pisa ^c, Pisa, Italy

K. Androsov^{a,30}, P. Azzurri^{a,15}, G. Bagliesi^a, J. Bernardini^a, T. Boccali^a, R. Castaldi^a, M.A. Ciocci^{a,30}, R. Dell'Orso^a, S. Donato^{a,c}, G. Fedi, A. Giassi^a, M.T. Grippo^{a,30}, F. Ligabue^{a,c}, T. Lomtadze^a, L. Martini^{a,b}, A. Messineo^{a,b}, F. Palla^a, A. Rizzi^{a,b}, A. Savoy-Navarro^{a,31}, P. Spagnolo^a, R. Tenchini^a, G. Tonelli^{a,b}, A. Venturi^a, P.G. Verdini^a

INFN Sezione di Roma ^a, Università di Roma ^b, Roma, Italy

L. Barone^{a,b}, F. Cavallari^a, M. Cipriani^{a,b}, G. D'imperio^{a,b,15}, D. Del Re^{a,b,15}, M. Diemoz^a, S. Gelli^{a,b}, C. Jorda^a, E. Longo^{a,b}, F. Margaroli^{a,b}, P. Meridiani^a, G. Organtini^{a,b}, R. Paramatti^a, F. Preiato^{a,b}, S. Rahatlou^{a,b}, C. Rovelli^a, F. Santanastasio^{a,b}

INFN Sezione di Torino ^a, Università di Torino ^b, Torino, Italy, Università del Piemonte Orientale ^c, Novara, Italy

N. Amapane^{a,b}, R. Arcidiacono^{a,c,15}, S. Argiro^{a,b}, M. Arneodo^{a,c}, N. Bartosik^a, R. Bellan^{a,b}, C. Biino^a, N. Cartiglia^a, M. Costa^{a,b}, R. Covarelli^{a,b}, A. Degano^{a,b}, N. Demaria^a, L. Finco^{a,b}, B. Kiani^{a,b}, C. Mariotti^a, S. Maselli^a, E. Migliore^{a,b}, V. Monaco^{a,b}, E. Monteil^{a,b}, M.M. Obertino^{a,b}, L. Pacher^{a,b}, N. Pastrone^a, M. Pelliccioni^a, G.L. Pinna Angioni^{a,b}, F. Ravera^{a,b}, A. Romero^{a,b}, M. Ruspa^{a,c}, R. Sacchi^{a,b}, K. Shchelina^{a,b}, V. Sola^a, A. Solano^{a,b}, A. Staiano^a, P. Traczyk^{a,b}

INFN Sezione di Trieste ^a, Università di Trieste ^b, Trieste, Italy

S. Belforte^a, V. Candelise^{a,b}, M. Casarsa^a, F. Cossutti^a, G. Della Ricca^{a,b}, C. La Licata^{a,b},
A. Schizzi^{a,b}, A. Zanetti^a

Kyungpook National University, Daegu, Korea

D.H. Kim, G.N. Kim, M.S. Kim, S. Lee, S.W. Lee, Y.D. Oh, S. Sekmen, D.C. Son, Y.C. Yang

Chonbuk National University, Jeonju, Korea

H. Kim, A. Lee

Hanyang University, Seoul, Korea

J.A. Brochero Cifuentes, T.J. Kim

Korea University, Seoul, Korea

S. Cho, S. Choi, Y. Go, D. Gyun, S. Ha, B. Hong, Y. Jo, Y. Kim, B. Lee, K. Lee, K.S. Lee, S. Lee,
J. Lim, S.K. Park, Y. Roh

Seoul National University, Seoul, Korea

J. Almond, J. Kim, S.B. Oh, S.h. Seo, U.K. Yang, H.D. Yoo, G.B. Yu

University of Seoul, Seoul, Korea

M. Choi, H. Kim, H. Kim, J.H. Kim, J.S.H. Lee, I.C. Park, G. Ryu, M.S. Ryu

Sungkyunkwan University, Suwon, Korea

Y. Choi, J. Goh, D. Kim, E. Kwon, J. Lee, I. Yu

Vilnius University, Vilnius, Lithuania

V. Dudenas, A. Juodagalvis, J. Vaitkus

National Centre for Particle Physics, Universiti Malaya, Kuala Lumpur, Malaysia

I. Ahmed, Z.A. Ibrahim, J.R. Komaragiri, M.A.B. Md Ali³², F. Mohamad Idris³³, W.A.T. Wan
Abdullah, M.N. Yusli, Z. Zolkapli

Centro de Investigacion y de Estudios Avanzados del IPN, Mexico City, Mexico

E. Casimiro Linares, H. Castilla-Valdez, E. De La Cruz-Burelo, I. Heredia-De La Cruz³⁴,
A. Hernandez-Almada, R. Lopez-Fernandez, J. Mejia Guisao, A. Sanchez-Hernandez

Universidad Iberoamericana, Mexico City, Mexico

S. Carrillo Moreno, F. Vazquez Valencia

Benemerita Universidad Autonoma de Puebla, Puebla, Mexico

I. Pedraza, H.A. Salazar Ibarguen, C. Uribe Estrada

Universidad Autónoma de San Luis Potosí, San Luis Potosí, Mexico

A. Morelos Pineda

University of Auckland, Auckland, New Zealand

D. Krofcheck

University of Canterbury, Christchurch, New Zealand

P.H. Butler

National Centre for Physics, Quaid-I-Azam University, Islamabad, Pakistan

A. Ahmad, M. Ahmad, Q. Hassan, H.R. Hoorani, W.A. Khan, T. Khurshid, M. Shoaib, M. Waqas

National Centre for Nuclear Research, Swierk, Poland

H. Bialkowska, M. Bluj, B. Boimska, T. Frueboes, M. Górski, M. Kazana, K. Nawrocki,
K. Romanowska-Rybinska, M. Szleper, P. Zalewski

Institute of Experimental Physics, Faculty of Physics, University of Warsaw, Warsaw, Poland
K. Bunkowski, A. Byzuk³⁵, K. Doroba, A. Kalinowski, M. Konecki, J. Krolikowski, M. Misiura, M. Olszewski, M. Walczak

Laboratório de Instrumentação e Física Experimental de Partículas, Lisboa, Portugal
P. Bargassa, C. Beirão Da Cruz E Silva, A. Di Francesco, P. Faccioli, P.G. Ferreira Parracho, M. Gallinaro, J. Hollar, N. Leonardo, L. Lloret Iglesias, M.V. Nemallapudi, J. Rodrigues Antunes, J. Seixas, O. Toldaiev, D. Vadrucchio, J. Varela, P. Vischia

Joint Institute for Nuclear Research, Dubna, Russia
P. Bunin, M. Gavrilenko, I. Golutvin, I. Gorbunov, V. Karjavin, A. Lanev, A. Malakhov, V. Matveev^{36,37}, P. Moisenz, V. Palichik, V. Perelygin, M. Savina, S. Shmatov, S. Shulha, N. Skatchkov, V. Smirnov, N. Voytishin, B.S. Yuldashev³⁸, A. Zarubin

Petersburg Nuclear Physics Institute, Gatchina (St. Petersburg), Russia
L. Chtchypounov, V. Golovtsov, Y. Ivanov, V. Kim³⁹, E. Kuznetsova⁴⁰, V. Murzin, V. Oreshkin, V. Sulimov, A. Vorobyev

Institute for Nuclear Research, Moscow, Russia
Yu. Andreev, A. Dermenev, S. Gninenko, N. Golubev, A. Karneyeu, M. Kirsanov, N. Krasnikov, A. Pashenkov, D. Tlisov, A. Toropin

Institute for Theoretical and Experimental Physics, Moscow, Russia
V. Epshteyn, V. Gavrillov, N. Lychkovskaya, V. Popov, I. Pozdnyakov, G. Safronov, A. Spiridonov, M. Toms, E. Vlasov, A. Zhokin

National Research Nuclear University 'Moscow Engineering Physics Institute' (MEPhI), Moscow, Russia
M. Chadeeva, M. Danilov, E. Tarkovskii

P.N. Lebedev Physical Institute, Moscow, Russia
V. Andreev, M. Azarkin³⁷, I. Dremin³⁷, M. Kirakosyan, A. Leonidov³⁷, S.V. Rusakov, A. Terkulov

Skobeltsyn Institute of Nuclear Physics, Lomonosov Moscow State University, Moscow, Russia
A. Baskakov, A. Belyaev, E. Boos, M. Dubinin⁴¹, L. Dudko, A. Ershov, A. Gribushin, V. Klyukhin, O. Kodolova, I. Lokhtin, I. Miagkov, S. Obraztsov, S. Petrushanko, V. Savrin, A. Snigirev

State Research Center of Russian Federation, Institute for High Energy Physics, Protvino, Russia
I. Azhgirey, I. Bayshev, S. Bitioukov, D. Elumakhov, V. Kachanov, A. Kalinin, D. Konstantinov, V. Krychkin, V. Petrov, R. Ryutin, A. Sobol, S. Troshin, N. Tyurin, A. Uzunian, A. Volkov

University of Belgrade, Faculty of Physics and Vinca Institute of Nuclear Sciences, Belgrade, Serbia
P. Adzic⁴², P. Cirkovic, D. Devetak, J. Milosevic, V. Rekovic

Centro de Investigaciones Energéticas Medioambientales y Tecnológicas (CIEMAT), Madrid, Spain
J. Alcaraz Maestre, E. Calvo, M. Cerrada, M. Chamizo Llatas, N. Colino, B. De La Cruz, A. Delgado Peris, A. Escalante Del Valle, C. Fernandez Bedoya, J.P. Fernández Ramos, J. Flix, M.C. Fouz, P. Garcia-Abia, O. Gonzalez Lopez, S. Goy Lopez, J.M. Hernandez, M.I. Josa,

E. Navarro De Martino, A. Pérez-Calero Yzquierdo, J. Puerta Pelayo, A. Quintario Olmeda, I. Redondo, L. Romero, M.S. Soares

Universidad Autónoma de Madrid, Madrid, Spain

J.F. de Trocóniz, M. Missiroli, D. Moran

Universidad de Oviedo, Oviedo, Spain

J. Cuevas, J. Fernandez Menendez, I. Gonzalez Caballero, E. Palencia Cortezon, S. Sanchez Cruz, J.M. Vizan Garcia

Instituto de Física de Cantabria (IFCA), CSIC-Universidad de Cantabria, Santander, Spain

I.J. Cabrillo, A. Calderon, J.R. Castiñeiras De Saa, E. Curras, M. Fernandez, J. Garcia-Ferrero, G. Gomez, A. Lopez Virto, J. Marco, C. Martinez Rivero, F. Matorras, J. Piedra Gomez, T. Rodrigo, A. Ruiz-Jimeno, L. Scodellaro, N. Trevisani, I. Vila, R. Vilar Cortabitarte

CERN, European Organization for Nuclear Research, Geneva, Switzerland

D. Abbaneo, E. Auffray, G. Auzinger, M. Bachtis, P. Baillon, A.H. Ball, D. Barney, P. Bloch, A. Bocci, A. Bonato, C. Botta, T. Camporesi, R. Castello, M. Cepeda, G. Cerminara, M. D'Alfonso, D. d'Enterria, A. Dabrowski, V. Daponte, A. David, M. De Gruttola, F. De Guio, A. De Roeck, E. Di Marco⁴³, M. Dobson, M. Dordevic, B. Dorney, T. du Pree, D. Duggan, M. Dünser, N. Dupont, A. Elliott-Peisert, S. Fartoukh, G. Franzoni, J. Fulcher, W. Funk, D. Gigi, K. Gill, M. Girone, F. Glege, S. Gundacker, M. Guthoff, J. Hammer, P. Harris, J. Hegeman, V. Innocente, P. Janot, H. Kirschenmann, V. Knünz, M.J. Kortelainen, K. Kousouris, M. Kramer¹, P. Lecoq, C. Lourenço, M.T. Lucchini, N. Magini, L. Malgeri, M. Mannelli, A. Martelli, F. Meijers, S. Mersi, E. Meschi, F. Moortgat, S. Morovic, M. Mulders, H. Neugebauer, S. Orfanelli⁴⁴, L. Orsini, L. Pape, E. Perez, M. Peruzzi, A. Petrilli, G. Petrucciani, A. Pfeiffer, M. Pierini, A. Racz, T. Reis, G. Rolandi⁴⁵, M. Rovere, M. Ruan, H. Sakulin, J.B. Sauvan, C. Schäfer, C. Schwick, M. Seidel, A. Sharma, P. Silva, M. Simon, P. Sphicas⁴⁶, J. Steggemann, M. Stoye, Y. Takahashi, D. Treille, A. Triossi, A. Tsirou, V. Veckalns⁴⁷, G.I. Veres²¹, N. Wardle, A. Zagozdzińska³⁵, W.D. Zeuner

Paul Scherrer Institut, Villigen, Switzerland

W. Bertl, K. Deiters, W. Erdmann, R. Horisberger, Q. Ingram, H.C. Kaestli, D. Kotlinski, U. Langenegger, T. Rohe

Institute for Particle Physics, ETH Zurich, Zurich, Switzerland

F. Bachmair, L. Bäni, L. Bianchini, B. Casal, G. Dissertori, M. Dittmar, M. Donegà, P. Eller, C. Grab, C. Heidegger, D. Hits, J. Hoss, G. Kasieczka, P. Lecomte[†], W. Lustermann, B. Mangano, M. Marionneau, P. Martinez Ruiz del Arbol, M. Masciovecchio, M.T. Meinhard, D. Meister, F. Micheli, P. Musella, F. Nessi-Tedaldi, F. Pandolfi, J. Pata, F. Pauss, G. Perrin, L. Perrozzi, M. Quittnat, M. Rossini, M. Schönenberger, A. Starodumov⁴⁸, M. Takahashi, V.R. Tavolaro, K. Theofilatos, R. Wallny

Universität Zürich, Zurich, Switzerland

T.K. Aarrestad, C. Amsler⁴⁹, L. Caminada, M.F. Canelli, V. Chiochia, A. De Cosa, C. Galloni, A. Hinzmann, T. Hreus, B. Kilminster, C. Lange, J. Ngadiuba, D. Pinna, G. Rauco, P. Robmann, D. Salerno, Y. Yang

National Central University, Chung-Li, Taiwan

T.H. Doan, Sh. Jain, R. Khurana, M. Konyushikhin, C.M. Kuo, W. Lin, Y.J. Lu, A. Pozdnyakov, S.S. Yu

National Taiwan University (NTU), Taipei, Taiwan

Arun Kumar, P. Chang, Y.H. Chang, Y.W. Chang, Y. Chao, K.F. Chen, P.H. Chen, C. Dietz,

F. Fiori, W.-S. Hou, Y. Hsiung, Y.F. Liu, R.-S. Lu, M. Miñano Moya, E. Paganis, A. Psallidas, J.f. Tsai, Y.M. Tzeng

Chulalongkorn University, Faculty of Science, Department of Physics, Bangkok, Thailand

B. Asavapibhop, G. Singh, N. Srimanobhas, N. Suwonjandee

Cukurova University, Adana, Turkey

A. Adiguzel, S. Cerci⁵⁰, S. Damarseckin, Z.S. Demiroglu, C. Dozen, I. Dumanoglu, S. Girgis, G. Gokbulut, Y. Guler, E. Gurpinar, I. Hos, E.E. Kangal⁵¹, A. Kayis Topaksu, G. Onengut⁵², K. Ozdemir⁵³, D. Sunar Cerci⁵⁰, B. Tali⁵⁰, C. Zorbilmez

Middle East Technical University, Physics Department, Ankara, Turkey

B. Bilin, S. Bilmis, B. Isildak⁵⁴, G. Karapinar⁵⁵, M. Yalvac, M. Zeyrek

Bogazici University, Istanbul, Turkey

E. Gülmez, M. Kaya⁵⁶, O. Kaya⁵⁷, E.A. Yetkin⁵⁸, T. Yetkin⁵⁹

Istanbul Technical University, Istanbul, Turkey

A. Cakir, K. Cankocak, S. Sen⁶⁰, F.I. Vardarli

Institute for Scintillation Materials of National Academy of Science of Ukraine, Kharkov, Ukraine

B. Grynyov

National Scientific Center, Kharkov Institute of Physics and Technology, Kharkov, Ukraine

L. Levchuk, P. Sorokin

University of Bristol, Bristol, United Kingdom

R. Aggleton, F. Ball, L. Beck, J.J. Brooke, D. Burns, E. Clement, D. Cussans, H. Flacher, J. Goldstein, M. Grimes, G.P. Heath, H.F. Heath, J. Jacob, L. Kreczko, C. Lucas, Z. Meng, D.M. Newbold⁶¹, S. Paramesvaran, A. Poll, T. Sakuma, S. Seif El Nasr-storey, S. Senkin, D. Smith, V.J. Smith

Rutherford Appleton Laboratory, Didcot, United Kingdom

K.W. Bell, A. Belyaev⁶², C. Brew, R.M. Brown, L. Calligaris, D. Cieri, D.J.A. Cockerill, J.A. Coughlan, K. Harder, S. Harper, E. Olaiya, D. Petyt, C.H. Shepherd-Themistocleous, A. Thea, I.R. Tomalin, T. Williams

Imperial College, London, United Kingdom

M. Baber, R. Bainbridge, O. Buchmuller, A. Bundock, D. Burton, S. Casasso, M. Citron, D. Colling, L. Corpe, P. Dauncey, G. Davies, A. De Wit, M. Della Negra, P. Dunne, A. Elwood, D. Futyan, Y. Haddad, G. Hall, G. Iles, R. Lane, C. Laner, R. Lucas⁶¹, L. Lyons, A.-M. Magnan, S. Malik, L. Mastrolorenzo, J. Nash, A. Nikitenko⁴⁸, J. Pela, B. Penning, M. Pesaresi, D.M. Raymond, A. Richards, A. Rose, C. Seez, A. Tapper, K. Uchida, M. Vazquez Acosta⁶³, T. Virdee¹⁵, S.C. Zenz

Brunel University, Uxbridge, United Kingdom

J.E. Cole, P.R. Hobson, A. Khan, P. Kyberd, D. Leslie, I.D. Reid, P. Symonds, L. Teodorescu, M. Turner

Baylor University, Waco, USA

A. Borzou, K. Call, J. Dittmann, K. Hatakeyama, H. Liu, N. Pastika

The University of Alabama, Tuscaloosa, USA

O. Charaf, S.I. Cooper, C. Henderson, P. Rumerio

Boston University, Boston, USA

D. Arcaro, A. Avetisyan, T. Bose, D. Gastler, D. Rankin, C. Richardson, J. Rohlf, L. Sulak, D. Zou

Brown University, Providence, USA

G. Benelli, E. Berry, D. Cutts, A. Ferapontov, A. Garabedian, J. Hakala, U. Heintz, O. Jesus, E. Laird, G. Landsberg, Z. Mao, M. Narain, S. Piperov, S. Sagir, E. Spencer, R. Syarif

University of California, Davis, Davis, USA

R. Breedon, G. Breto, D. Burns, M. Calderon De La Barca Sanchez, S. Chauhan, M. Chertok, J. Conway, R. Conway, P.T. Cox, R. Erbacher, C. Flores, G. Funk, M. Gardner, W. Ko, R. Lander, C. Mclean, M. Mulhearn, D. Pellett, J. Pilot, F. Ricci-Tam, S. Shalhout, J. Smith, M. Squires, D. Stolp, M. Tripathi, S. Wilbur, R. Yohay

University of California, Los Angeles, USA

R. Cousins, P. Everaerts, A. Florent, J. Hauser, M. Ignatenko, D. Saltzberg, E. Takasugi, V. Valuev, M. Weber

University of California, Riverside, Riverside, USA

K. Burt, R. Clare, J. Ellison, J.W. Gary, G. Hanson, J. Heilman, P. Jandir, E. Kennedy, F. Lacroix, O.R. Long, M. Malberti, M. Olmedo Negrete, M.I. Paneva, A. Shrinivas, H. Wei, S. Wimpenny, B. R. Yates

University of California, San Diego, La Jolla, USA

J.G. Branson, G.B. Cerati, S. Cittolin, R.T. D'Agnolo, M. Derdzinski, R. Gerosa, A. Holzner, R. Kelley, D. Klein, J. Letts, I. Macneill, D. Olivito, S. Padhi, M. Pieri, M. Sani, V. Sharma, S. Simon, M. Tadel, A. Vartak, S. Wasserbaech⁶⁴, C. Welke, J. Wood, F. Würthwein, A. Yagil, G. Zevi Della Porta

University of California, Santa Barbara, Santa Barbara, USA

R. Bhandari, J. Bradmiller-Feld, C. Campagnari, A. Dishaw, V. Dutta, K. Flowers, M. Franco Sevilla, P. Geffert, C. George, F. Golf, L. Gouskos, J. Gran, R. Heller, J. Incandela, N. Mccoll, S.D. Mullin, A. Ovcharova, J. Richman, D. Stuart, I. Suarez, C. West, J. Yoo

California Institute of Technology, Pasadena, USA

D. Anderson, A. Apresyan, J. Bendavid, A. Bornheim, J. Bunn, Y. Chen, J. Duarte, A. Mott, H.B. Newman, C. Pena, M. Spiropulu, J.R. Vlimant, S. Xie, R.Y. Zhu

Carnegie Mellon University, Pittsburgh, USA

M.B. Andrews, V. Azzolini, A. Calamba, B. Carlson, T. Ferguson, M. Paulini, J. Russ, M. Sun, H. Vogel, I. Vorobiev

University of Colorado Boulder, Boulder, USA

J.P. Cumalat, W.T. Ford, F. Jensen, A. Johnson, M. Krohn, T. Mulholland, K. Stenson, S.R. Wagner

Cornell University, Ithaca, USA

J. Alexander, J. Chaves, J. Chu, S. Dittmer, N. Mirman, G. Nicolas Kaufman, J.R. Patterson, A. Rinkevicius, A. Ryd, L. Skinnari, W. Sun, S.M. Tan, Z. Tao, J. Thom, J. Tucker, P. Wittich

Fairfield University, Fairfield, USA

D. Winn

Fermi National Accelerator Laboratory, Batavia, USA

S. Abdullin, M. Albrow, G. Apollinari, S. Banerjee, L.A.T. Bauerdick, A. Beretvas, J. Berryhill, P.C. Bhat, G. Bolla, K. Burkett, J.N. Butler, H.W.K. Cheung, F. Chlebana, S. Cihangir,

M. Cremonesi, V.D. Elvira, I. Fisk, J. Freeman, E. Gottschalk, L. Gray, D. Green, S. Grünendahl, O. Gutsche, D. Hare, R.M. Harris, S. Hasegawa, J. Hirschauer, Z. Hu, B. Jayatilaka, S. Jindariani, M. Johnson, U. Joshi, B. Klima, B. Kreis, S. Lammel, J. Linacre, D. Lincoln, R. Lipton, T. Liu, R. Lopes De Sá, J. Lykken, K. Maeshima, J.M. Marraffino, S. Maruyama, D. Mason, P. McBride, P. Merkel, S. Mrenna, S. Nahn, C. Newman-Holmes[†], V. O'Dell, K. Pedro, O. Prokofyev, G. Rakness, L. Ristori, E. Sexton-Kennedy, A. Soha, W.J. Spalding, L. Spiegel, S. Stoynev, N. Strobbe, L. Taylor, S. Tkaczyk, N.V. Tran, L. Uplegger, E.W. Vaandering, C. Vernieri, M. Verzocchi, R. Vidal, M. Wang, H.A. Weber, A. Whitbeck

University of Florida, Gainesville, USA

D. Acosta, P. Avery, P. Bortignon, D. Bourilkov, A. Brinkerhoff, A. Carnes, M. Carver, D. Curry, S. Das, R.D. Field, I.K. Furic, J. Konigsberg, A. Korytov, P. Ma, K. Matchev, H. Mei, P. Milenovic⁶⁵, G. Mitselmakher, D. Rank, L. Shchutska, D. Sperka, L. Thomas, J. Wang, S. Wang, J. Yelton

Florida International University, Miami, USA

S. Linn, P. Markowitz, G. Martinez, J.L. Rodriguez

Florida State University, Tallahassee, USA

A. Ackert, J.R. Adams, T. Adams, A. Askew, S. Bein, B. Diamond, S. Hagopian, V. Hagopian, K.F. Johnson, A. Khatiwada, H. Prosper, A. Santra, M. Weinberg

Florida Institute of Technology, Melbourne, USA

M.M. Baarmand, V. Bhopatkar, S. Colafranceschi⁶⁶, M. Hohlmann, H. Kalakhety, D. Noonan, T. Roy, F. Yumiceva

University of Illinois at Chicago (UIC), Chicago, USA

M.R. Adams, L. Apanasevich, D. Berry, R.R. Betts, I. Bucinskaite, R. Cavanaugh, O. Evdokimov, L. Gauthier, C.E. Gerber, D.J. Hofman, P. Kurt, C. O'Brien, I.D. Sandoval Gonzalez, P. Turner, N. Varelas, Z. Wu, M. Zakaria, J. Zhang

The University of Iowa, Iowa City, USA

B. Bilki⁶⁷, W. Clarida, K. Dilsiz, S. Durgut, R.P. Gandrajula, M. Haytmyradov, V. Khristenko, J.-P. Merlo, H. Mermerkaya⁶⁸, A. Mestvirishvili, A. Moeller, J. Nachtman, H. Ogul, Y. Onel, F. Ozok⁶⁹, A. Penzo, C. Snyder, E. Tiras, J. Wetzel, K. Yi

Johns Hopkins University, Baltimore, USA

I. Anderson, B. Blumenfeld, A. Cocoros, N. Eminizer, D. Fehling, L. Feng, A.V. Gritsan, P. Maksimovic, M. Osherson, J. Roskes, U. Sarica, M. Swartz, M. Xiao, Y. Xin, C. You

The University of Kansas, Lawrence, USA

A. Al-bataineh, P. Baringer, A. Bean, J. Bowen, C. Bruner, J. Castle, R.P. Kenny III, A. Kropivnitskaya, D. Majumder, W. Mcbrayer, M. Murray, S. Sanders, R. Stringer, J.D. Tapia Takaki, Q. Wang

Kansas State University, Manhattan, USA

A. Ivanov, K. Kaadze, S. Khalil, M. Makouski, Y. Maravin, A. Mohammadi, L.K. Saini, N. Skhirtladze, S. Toda

Lawrence Livermore National Laboratory, Livermore, USA

D. Lange, F. Rebassoo, D. Wright

University of Maryland, College Park, USA

C. Anelli, A. Baden, O. Baron, A. Belloni, B. Calvert, S.C. Eno, C. Ferraioli, J.A. Gomez,

N.J. Hadley, S. Jabeen, R.G. Kellogg, T. Kolberg, J. Kunkle, Y. Lu, A.C. Mignerey, Y.H. Shin, A. Skuja, M.B. Tonjes, S.C. Tonwar

Massachusetts Institute of Technology, Cambridge, USA

A. Apyan, R. Barbieri, A. Baty, R. Bi, K. Bierwagen, S. Brandt, W. Busza, I.A. Cali, Z. Demiragli, L. Di Matteo, G. Gomez Ceballos, M. Goncharov, D. Gulhan, D. Hsu, Y. Iiyama, G.M. Innocenti, M. Klute, D. Kovalskyi, K. Krajczar, Y.S. Lai, Y.-J. Lee, A. Levin, P.D. Luckey, A.C. Marini, C. McGinn, C. Mironov, S. Narayanan, X. Niu, C. Paus, C. Roland, G. Roland, J. Salfeld-Nebgen, G.S.F. Stephans, K. Sumorok, K. Tatar, M. Varma, D. Velicanu, J. Veverka, J. Wang, T.W. Wang, B. Wyslouch, M. Yang, V. Zhukova

University of Minnesota, Minneapolis, USA

A.C. Benvenuti, R.M. Chatterjee, B. Dahmes, A. Evans, A. Finkel, A. Gude, P. Hansen, S. Kalafut, S.C. Kao, K. Klapoetke, Y. Kubota, Z. Lesko, J. Mans, S. Nourbakhsh, N. Ruckstuhl, R. Rusack, N. Tambe, J. Turkewitz

University of Mississippi, Oxford, USA

J.G. Acosta, S. Oliveros

University of Nebraska-Lincoln, Lincoln, USA

E. Avdeeva, R. Bartek, K. Bloom, S. Bose, D.R. Claes, A. Dominguez, C. Fangmeier, R. Gonzalez Suarez, R. Kamalieddin, D. Knowlton, I. Kravchenko, F. Meier, J. Monroy, J.E. Siado, G.R. Snow, B. Stieger

State University of New York at Buffalo, Buffalo, USA

M. Alyari, J. Dolen, J. George, A. Godshalk, C. Harrington, I. Iashvili, J. Kaisen, A. Kharchilava, A. Kumar, A. Parker, S. Rappoccio, B. Roozbahani

Northeastern University, Boston, USA

G. Alverson, E. Barberis, D. Baumgartel, M. Chasco, A. Hortiangtham, A. Massironi, D.M. Morse, D. Nash, T. Orimoto, R. Teixeira De Lima, D. Trocino, R.-J. Wang, D. Wood

Northwestern University, Evanston, USA

S. Bhattacharya, K.A. Hahn, A. Kubik, J.F. Low, N. Mucia, N. Odell, B. Pollack, M.H. Schmitt, K. Sung, M. Trovato, M. Velasco

University of Notre Dame, Notre Dame, USA

N. Dev, M. Hildreth, K. Hurtado Anampa, C. Jessop, D.J. Karmgard, N. Kellams, K. Lannon, N. Marinelli, F. Meng, C. Mueller, Y. Musienko³⁶, M. Planer, A. Reinsvold, R. Ruchti, N. Rupperecht, G. Smith, S. Taroni, N. Valls, M. Wayne, M. Wolf, A. Woodard

The Ohio State University, Columbus, USA

J. Alimena, L. Antonelli, J. Brinson, B. Bylsma, L.S. Durkin, S. Flowers, B. Francis, A. Hart, C. Hill, R. Hughes, W. Ji, B. Liu, W. Luo, D. Puigh, M. Rodenburg, B.L. Winer, H.W. Wulsin

Princeton University, Princeton, USA

S. Cooperstein, O. Driga, P. Elmer, J. Hardenbrook, P. Hebda, J. Luo, D. Marlow, T. Medvedeva, M. Mooney, J. Olsen, C. Palmer, P. Piroué, D. Stickland, C. Tully, A. Zuranski

University of Puerto Rico, Mayaguez, USA

S. Malik

Purdue University, West Lafayette, USA

A. Barker, V.E. Barnes, D. Benedetti, S. Folgueras, L. Gutay, M.K. Jha, M. Jones, A.W. Jung,

K. Jung, D.H. Miller, N. Neumeister, B.C. Radburn-Smith, X. Shi, J. Sun, A. Svyatkovskiy, F. Wang, W. Xie, L. Xu

Purdue University Calumet, Hammond, USA

N. Parashar, J. Stupak

Rice University, Houston, USA

A. Adair, B. Akgun, Z. Chen, K.M. Ecklund, F.J.M. Geurts, M. Guilbaud, W. Li, B. Michlin, M. Northup, B.P. Padley, R. Redjimi, J. Roberts, J. Rorie, Z. Tu, J. Zabel

University of Rochester, Rochester, USA

B. Betchart, A. Bodek, P. de Barbaro, R. Demina, Y.t. Duh, T. Ferbel, M. Galanti, A. Garcia-Bellido, J. Han, O. Hindrichs, A. Khukhunaishvili, K.H. Lo, P. Tan, M. Verzetti

Rutgers, The State University of New Jersey, Piscataway, USA

J.P. Chou, E. Contreras-Campana, Y. Gershtein, T.A. Gómez Espinosa, E. Halkiadakis, M. Heindl, D. Hidas, E. Hughes, S. Kaplan, R. Kunnawalkam Elayavalli, S. Kyriacou, A. Lath, K. Nash, H. Saka, S. Salur, S. Schnetzer, D. Sheffield, S. Somalwar, R. Stone, S. Thomas, P. Thomassen, M. Walker

University of Tennessee, Knoxville, USA

M. Foerster, J. Heideman, G. Riley, K. Rose, S. Spanier, K. Thapa

Texas A&M University, College Station, USA

O. Bouhali⁷⁰, A. Castaneda Hernandez⁷⁰, A. Celik, M. Dalchenko, M. De Mattia, A. Delgado, S. Dildick, R. Eusebi, J. Gilmore, T. Huang, E. Juska, T. Kamon⁷¹, V. Krutelyov, R. Mueller, Y. Pakhotin, R. Patel, A. Perloff, L. Perniè, D. Rathjens, A. Rose, A. Safonov, A. Tatarinov, K.A. Ulmer

Texas Tech University, Lubbock, USA

N. Akchurin, C. Cowden, J. Damgov, C. Dragoiu, P.R. Duderu, J. Faulkner, S. Kunori, K. Lamichhane, S.W. Lee, T. Libeiro, S. Undleeb, I. Volobouev, Z. Wang

Vanderbilt University, Nashville, USA

A.G. Delannoy, S. Greene, A. Gurrola, R. Janjam, W. Johns, C. Maguire, A. Melo, H. Ni, P. Sheldon, S. Tuo, J. Velkovska, Q. Xu

University of Virginia, Charlottesville, USA

M.W. Arenton, P. Barria, B. Cox, J. Goodell, R. Hirosky, A. Ledovskoy, H. Li, C. Neu, T. Sinthuprasith, X. Sun, Y. Wang, E. Wolfe, F. Xia

Wayne State University, Detroit, USA

C. Clarke, R. Harr, P.E. Karchin, P. Lamichhane, J. Sturdy

University of Wisconsin - Madison, Madison, WI, USA

D.A. Belknap, S. Dasu, L. Dodd, S. Duric, B. Gomber, M. Grothe, M. Herndon, A. Hervé, P. Klabbers, A. Lanaro, A. Levine, K. Long, R. Loveless, I. Ojalvo, T. Perry, G.A. Pierro, G. Polese, T. Ruggles, A. Savin, A. Sharma, N. Smith, W.H. Smith, D. Taylor, P. Verwilligen, N. Woods

†: Deceased

1: Also at Vienna University of Technology, Vienna, Austria

2: Also at State Key Laboratory of Nuclear Physics and Technology, Peking University, Beijing, China

3: Also at Institut Pluridisciplinaire Hubert Curien, Université de Strasbourg, Université de

-
- Haute Alsace Mulhouse, CNRS/IN2P3, Strasbourg, France
- 4: Also at Universidade Estadual de Campinas, Campinas, Brazil
 - 5: Also at Centre National de la Recherche Scientifique (CNRS) - IN2P3, Paris, France
 - 6: Also at Université Libre de Bruxelles, Bruxelles, Belgium
 - 7: Also at Deutsches Elektronen-Synchrotron, Hamburg, Germany
 - 8: Also at Joint Institute for Nuclear Research, Dubna, Russia
 - 9: Also at Helwan University, Cairo, Egypt
 - 10: Now at Zewail City of Science and Technology, Zewail, Egypt
 - 11: Also at Ain Shams University, Cairo, Egypt
 - 12: Also at Fayoum University, El-Fayoum, Egypt
 - 13: Also at British University in Egypt, Cairo, Egypt
 - 14: Also at Université de Haute Alsace, Mulhouse, France
 - 15: Also at CERN, European Organization for Nuclear Research, Geneva, Switzerland
 - 16: Also at Skobeltsyn Institute of Nuclear Physics, Lomonosov Moscow State University, Moscow, Russia
 - 17: Also at RWTH Aachen University, III. Physikalisches Institut A, Aachen, Germany
 - 18: Also at University of Hamburg, Hamburg, Germany
 - 19: Also at Brandenburg University of Technology, Cottbus, Germany
 - 20: Also at Institute of Nuclear Research ATOMKI, Debrecen, Hungary
 - 21: Also at MTA-ELTE Lendület CMS Particle and Nuclear Physics Group, Eötvös Loránd University, Budapest, Hungary
 - 22: Also at University of Debrecen, Debrecen, Hungary
 - 23: Also at Indian Institute of Science Education and Research, Bhopal, India
 - 24: Also at Institute of Physics, Bhubaneswar, India
 - 25: Also at University of Visva-Bharati, Santiniketan, India
 - 26: Also at University of Ruhuna, Matara, Sri Lanka
 - 27: Also at Isfahan University of Technology, Isfahan, Iran
 - 28: Also at University of Tehran, Department of Engineering Science, Tehran, Iran
 - 29: Also at Plasma Physics Research Center, Science and Research Branch, Islamic Azad University, Tehran, Iran
 - 30: Also at Università degli Studi di Siena, Siena, Italy
 - 31: Also at Purdue University, West Lafayette, USA
 - 32: Also at International Islamic University of Malaysia, Kuala Lumpur, Malaysia
 - 33: Also at Malaysian Nuclear Agency, MOSTI, Kajang, Malaysia
 - 34: Also at Consejo Nacional de Ciencia y Tecnología, Mexico city, Mexico
 - 35: Also at Warsaw University of Technology, Institute of Electronic Systems, Warsaw, Poland
 - 36: Also at Institute for Nuclear Research, Moscow, Russia
 - 37: Now at National Research Nuclear University 'Moscow Engineering Physics Institute' (MEPhI), Moscow, Russia
 - 38: Also at Institute of Nuclear Physics of the Uzbekistan Academy of Sciences, Tashkent, Uzbekistan
 - 39: Also at St. Petersburg State Polytechnical University, St. Petersburg, Russia
 - 40: Also at University of Florida, Gainesville, USA
 - 41: Also at California Institute of Technology, Pasadena, USA
 - 42: Also at Faculty of Physics, University of Belgrade, Belgrade, Serbia
 - 43: Also at INFN Sezione di Roma; Università di Roma, Roma, Italy
 - 44: Also at National Technical University of Athens, Athens, Greece
 - 45: Also at Scuola Normale e Sezione dell'INFN, Pisa, Italy
 - 46: Also at National and Kapodistrian University of Athens, Athens, Greece

-
- 47: Also at Riga Technical University, Riga, Latvia
 - 48: Also at Institute for Theoretical and Experimental Physics, Moscow, Russia
 - 49: Also at Albert Einstein Center for Fundamental Physics, Bern, Switzerland
 - 50: Also at Adiyaman University, Adiyaman, Turkey
 - 51: Also at Mersin University, Mersin, Turkey
 - 52: Also at Cag University, Mersin, Turkey
 - 53: Also at Piri Reis University, Istanbul, Turkey
 - 54: Also at Ozyegin University, Istanbul, Turkey
 - 55: Also at Izmir Institute of Technology, Izmir, Turkey
 - 56: Also at Marmara University, Istanbul, Turkey
 - 57: Also at Kafkas University, Kars, Turkey
 - 58: Also at Istanbul Bilgi University, Istanbul, Turkey
 - 59: Also at Yildiz Technical University, Istanbul, Turkey
 - 60: Also at Hacettepe University, Ankara, Turkey
 - 61: Also at Rutherford Appleton Laboratory, Didcot, United Kingdom
 - 62: Also at School of Physics and Astronomy, University of Southampton, Southampton, United Kingdom
 - 63: Also at Instituto de Astrofísica de Canarias, La Laguna, Spain
 - 64: Also at Utah Valley University, Orem, USA
 - 65: Also at University of Belgrade, Faculty of Physics and Vinca Institute of Nuclear Sciences, Belgrade, Serbia
 - 66: Also at Facoltà Ingegneria, Università di Roma, Roma, Italy
 - 67: Also at Argonne National Laboratory, Argonne, USA
 - 68: Also at Erzincan University, Erzincan, Turkey
 - 69: Also at Mimar Sinan University, Istanbul, Istanbul, Turkey
 - 70: Also at Texas A&M University at Qatar, Doha, Qatar
 - 71: Also at Kyungpook National University, Daegu, Korea